Heterochromatin-Associated Proteins HP1a and Piwi Collaborate to Maintain the Association of Achiasmate Homologs in *Drosophila* Oocytes

Christopher C. Giauque and Sharon E. Bickel[1]
Department of Biological Sciences, Dartmouth College, Hanover, New Hampshire 03755

ABSTRACT Accurate segregation of homologous chromosomes during meiosis depends on their ability to remain physically connected throughout prophase I. For homologs that achieve a crossover, sister chromatid cohesion distal to the chiasma keeps them attached until anaphase I. However, in *Drosophila melanogaster* wild-type oocytes, chromosome *4* never recombines, and the *X* chromosome fails to cross over in 6–10% of oocytes. Proper segregation of these achiasmate homologs relies on their pericentric heterochromatin-mediated association, but the mechanism(s) underlying this attachment remains poorly understood. Using an inducible RNA interference (RNAi) strategy combined with fluorescence *in situ* hybridization (FISH) to monitor centromere proximal association of the achiasmate *FM7a/X* homolog pair, we asked whether specific heterochromatin-associated proteins are required for the association and proper segregation of achiasmate homologs in *Drosophila* oocytes. When we knock down HP1a, H3K9 methytransferases, or the HP1a binding partner Piwi during mid-prophase, we observe significant disruption of pericentric heterochromatin-mediated association of *FM7a/X* homologs. Furthermore, for both HP1a and Piwi knockdown oocytes, transgenic coexpression of the corresponding wild-type protein is able to rescue RNAi-induced defects, but expression of a mutant protein with a single amino acid change that disrupts the HP1a-Piwi interaction is unable to do so. We show that Piwi is stably bound to numerous sites along the meiotic chromosomes, including centromere proximal regions. In addition, reduction of HP1a or Piwi during meiotic prophase induces a significant increase in *FM7a/X* segregation errors. We present a speculative model outlining how HP1a and Piwi could collaborate to keep achiasmate chromosomes associated in a homology-dependent manner.

KEYWORDS meiosis; chromosome segregation; H3K9 methyltransferases; pericentric heterochromatin; nondisjunction

ONE unique feature of meiosis is segregation of homologous chromosomes during the first division followed by segregation of sisters during meiosis II. For their proper segregation, homologs need to find each other and physically associate during meiotic prophase I. Prolonged association of homologous chromosomes is essential for establishing biorientation of their centromeres and proper microtubule attachments on the meiosis I spindle. If their association is not maintained, homologs are free to attach to microtubules emanating from the same pole, which can lead to nondisjunction and the production of aneuploid gametes. A crossover between homologous chromosomes is normally sufficient to ensure their accurate segregation because sister chromatid cohesion distal to the chiasma keeps the pair of recombinant homologs physically attached until anaphase I (Buonomo *et al.* 2000; Bickel *et al.* 2002; Hodges *et al.* 2005).

In the *Drosophila* oocyte, the *X* chromosome fails to cross over 6–10% of the time, and chromosome *4* never recombines (Ashburner *et al.* 2005). Still, these achiasmate chromosomes segregate faithfully in wild-type oocytes (Grell 1976). Elegant genetic experiments have uncovered the existence of a backup system in *Drosophila* oocytes that ensures proper segregation of homologs that lack a crossover and that is distinct from the achiasmate pathway that operates in the male germline (Theurkauf and Hawley 1992; Hawley *et al.* 1993; Whyte *et al.* 1993; Moore *et al.* 1994; Karpen *et al.* 1996). Accurate segregation of achiasmate homologs in *Drosophila* oocytes requires homology-dependent interactions within their pericentric heterochromatin (Hawley *et al.* 1993; Karpen

doi: 10.1534/genetics.115.186460
Manuscript received December 22, 2015; accepted for publication March 11, 2016; published Early Online March 15, 2016.
Supplemental material is available online at www.genetics.org/cgi/data/genetics.115.186460/DC1/.
[1]Corresponding author: Department of Biological Sciences, Dartmouth College, 78 College Street, Hanover, NH 03755. E-mail: sharon.e.bickel@dartmouth.edu

et al. 1996). Pericentric heterochromatin-mediated association of achiasmate homologs (for which we have adopted the acronym PHeMAAH) persists throughout prophase I (Dernburg *et al.* 1996), and heterochromatic threads connecting homologs have been visualized in oocytes during prometaphase I congression (Hughes *et al.* 2009). Models to explain how achiasmate homologs remain physically associated include the possibility of heterochromatin entanglements (Hughes *et al.* 2009) as well as heterochromatin-bound proteins acting to connect the two homologs (Karpen *et al.* 1996). Although a role for pericentric heterochromatin in PHeMAAH is well established, the function of heterochromatin proteins in this process remains largely unexplored.

HP1a, an essential heterochromatin protein encoded by the *Drosophila Su(var)205* gene, is enriched in pericentric heterochromatin (James *et al.* 1989), making it an attractive candidate for participation in PHeMAAH. HP1a is highly conserved, and functional orthologs in other species are also required for proper heterochromatin structure and function (Vermaak and Malik 2009; Zeng *et al.* 2010a; Canzio *et al.* 2014). The N-terminal chromodomain of HP1a binds to the canonical H3K9me2/3 heterochromatin mark, while its chromo shadow domain (CSD) at the C-terminus mediates the formation of homodimers (Mendez *et al.* 2011). *In vitro* experiments have demonstrated that HP1 dimers can interact with two nonadjacent nucleosomes within a multinucleosomal array (Canzio *et al.* 2011) or serve as a bridge between two independent nucleosomal arrays (Azzaz *et al.* 2014). In addition, when HP1a is tethered to a specific chromosomal site within *Drosophila* polytene chromosomes, its interaction with a distant location on the chromosome promotes looping (Azzaz *et al.* 2014). HP1a-mediated nucleosome-nucleosome interactions are thought to be critical in establishing and maintaining the compact structure of heterochromatin. Another key feature of the HP1a dimer is the binding surface created when its two CSDs come together, and this interaction platform is able to recruit additional proteins to the heterochromatin, including the nuclear protein Piwi (Mendez *et al.* 2013).

Piwi, a member of the Argonaute superfamily of proteins, is best known for its ability to bind Piwi-interacting RNAs (piRNAs) and prevent transposon mobilization in the germline (Mani and Juliano 2013; Ku and Lin 2014). Most piRNA sequences in the *Drosophila* genome map to heterochromatic regions (Saito *et al.* 2006), and several lines of investigation have demonstrated that Piwi and HP1a can physically interact (Brower-Toland *et al.* 2007; Mendez *et al.* 2011). Moreover, transcriptional silencing of retrotransposons by the Piwi-piRNA system involves recruitment of HP1a to transposable elements (Wang and Elgin 2011; Sentmanat and Elgin 2012; Huang *et al.* 2013). Piwi also participates in activities that are not directly related to transposon silencing. In the early *Drosophila* embryo, maternally inherited Piwi protein is required for localization of HP1a to specific genomic regions and subsequent establishment of heterochromatin at those locations (Gu and Elgin 2013). Piwi also has been implicated in a phenomenon termed *pairing-sensitive silencing*, in which "crosstalk" between homologs results in transcriptional repression of two transgenes on homologous chromosomes, but only when the transgenes are paired (Grimaud *et al.* 2006). The involvement of Piwi in heterochromatin formation and its role in facilitating communication between paired homologs raise the possibility that Piwi also may promote PHeMAAH in the *Drosophila* oocyte.

Here we explore a potential role for HP1a and Piwi in maintaining the association of achiasmate homologs during meiotic prophase I. We find that reduction of either protein in the oocyte disrupts PHeMAAH and causes achiasmate chromosomes to missegregate. Significantly, we find that the ability of HP1a and Piwi to promote PHeMAAH depends on their ability to interact with each other. We provide a speculative model for how these two heterochromatin localized proteins could collaborate to keep the pericentric heterochromatin of achiasmate homologs physically associated in a homology-dependent manner.

Materials and Methods

Fly stocks

Flies were raised on standard cornmeal/molasses food at 25°. Stocks containing a wild-type or mutant V30A Piwi transgene were provided by S. Elgin (Brower-Toland *et al.* 2007). All other fly stocks were obtained from Bloomington *Drosophila* Stock Center at Indiana University, the Vienna *Drosophila* RNAi Center, and the Harvard Transgenic RNAi Project or generated for this study (Supplemental Material, Table S1 provides a complete list of stocks and their sources). The *Su(var)205*^{5} allele has been characterized previously (Eissenberg *et al.* 1992), and the GFP-HP1a transgenic construct containing the native *Su(var)205* promoter is derived from the previously described RFP-HP1a transgene (Wen *et al.* 2008; Lipsick 2010).

Nondisjunction tests

Because *Drosophila* tolerate certain sex chromosome aneuploidies (*XXY* and *XO*), we can assay meiotic nondisjunction (NDJ) in females by using *X* chromosome markers that allow us to visually distinguish progeny arising from normal *X* chromosome segregation and exceptional progeny for which *X* chromosome missegregation resulted in diplo-*X* or nullo-*X* oocytes. To accommodate the visible markers carried on specific transgenes, we used two slightly different cross schemes to measure nondisjunction (Figure S1). For HP1a mutant and HP1a RNAi NDJ tests, *FM7a/y* females were crossed to attached *X^Y, v f B* males, and progeny were scored based on sex and body color. For Piwi RNAi NDJ tests, *FM7a/w B* females were crossed to males with attached *X^Y* chromosomes that carried a wild-type *Bar* allele, and progeny were scored based on sex and eye morphology. In both cross schemes, all the normal progeny but only half the exceptional progeny are expected to survive (*XXX^Y* and *00* are lethal), so total %NDJ was calculated as

$\{[2 \times (\text{diplos} + \text{nullos})]/(n + \text{diplos} + \text{nullos})\} \times 100$, where n is the total number of progeny scored. *P*-values were calculated using the method described in Zeng *et al.* (2010b).

Creation of GFP-HP1a constructs

Site-directed mutagenesis was used (Agilent QuikChange II Kit) to introduce silent mutations into the enhanced green fluorescent protein (EGFP) complementary DNA (cDNA) sequence in pEGFP-C1 (Clontech Laboratories) in order to remove *Kpn*I, *Bam*HI, and *Xba*I sites from the coding sequence and facilitate downstream cloning. During PCR amplification of EGFP, a short linker sequence encoding four amino acids was introduced at the 3′ end of the open reading frame (ORF), as well as *Eag*I and *Spe*I restriction sites flanking the ORF, which were used to clone the PCR product into the pUASP-attB vector (Takeo *et al.* 2012). Full-length HP1a cDNA (LD10408) in pBluescript SK(−) was obtained from the *Drosophila* Genome Resource Center and used as a template for site-directed mutagenesis to create a W200A mutant HP1a construct in the SK vector. The wild-type and W200A HP1a clones were used as PCR templates to generate HP1a ORF amplicons lacking the 3′ UTR (thereby conferring HP1a RNAi^{V20} resistance), and each was inserted downstream of EGFP in pUASP. Table S2 contains the sequences of all primers used for site-directed mutagenesis and cloning. The EGFP-HP1a inserts were excised from pUASP-attB and inserted into the pUAST-attB vector (Bischof *et al.* 2007) using *Eag*I and *Xba*I. All clones were verified by sequencing, and transgenic flies with insertions at the attP40 site on chromosome *2* were generated by Genetic Services, Inc. (Cambridge, MA).

For each insertion, a series of crosses was performed to generate a stock carrying both the GFP-HP1a transgene (chromosome *2*) and the HP1a RNAi^{V20} transgene (chromosome *3*). Expression of pUASP and pUAST versions of wild-type HP1a insertions was tested in fluorescence *in situ* hybridization (FISH) experiments, but preliminary results indicated that the pUAST resulted in more robust rescue of the HP1a knockdown (KD) phenotype; therefore, pUAST insertions were used for subsequent experiments.

Immunoblotting

Flies were fattened for 2–3 days on yeast, and ovaries from 20 females were dissected in 1× PBS, frozen in liquid nitrogen, and stored at −80° until ready to use. Frozen ovaries were homogenized in a solution of 8 M urea, 2% SDS, 100 mM Tris HCl (pH 6.8), 5% Ficoll, and 2 mM Pefabloc (Sigma-Aldrich), heated at 95° for 5 min, and centrifuged at 13,000 rpm for 5 min to pellet debris. The supernatant was transferred to a new tube, and protein concentration was quantified using the Bio-Rad DC protein assay. Then 15 μg of protein per lane (for HP1a blots) or 25 μg protein per lane (for Piwi blots) was separated on a Bio-Rad Mini-PROTEAN TGX Stain-Free 4–20% Gradient Gel and transferred to a Millipore PVDF membrane using a Bio-Rad Trans-Blot SD Semi-Dry apparatus. HP1a blots were cut at 37 kDa to allow separate processing of HP1a and tubulin bands. Each blot was stained with rabbit α-Piwi 1:5000 (Klattenhoff *et al.* 2009), rabbit α-HP1a 1:5000 (Covance PRC-291C), or monoclonal mouse α-tubulin 1:1000 (DM1A, Sigma T9206). After incubation with Promega AP-conjugated secondary antibodies diluted 1:7500, Lumi-Phos reagent (Thermo Scientific) or Immuno-Star AP substrate (Bio-Rad) was applied to the blots, and they were imaged on a Bio-Rad ChemiDoc Touch System. Signal intensity was quantified with Bio-Rad Image Lab 5.2.1 software. HP1a bands were normalized to the tubulin signal, and the normalized KD signal was divided by the normalized control signal to determine relative protein amount. Because Piwi KD ovaries were consistently smaller than control ovaries, we were concerned that normalization using tubulin might not be accurate. Therefore, for Piwi blots, we used Bio-Rad Stain-Free Gel Technology to quantify the total protein signal in each lane of the blot and then normalized the Piwi band intensity to the total protein in each lane. Normalized KD signal was divided by the normalized control signal to quantify Piwi knockdown.

Fluorescence in situ hybridization (FISH)

Ovaries were probed using a Cy3-labeled oligo (5′-Cy3-AGGGATCGTTAGCACTCGTAAT; Integrated DNA Technologies) that corresponds to a portion of the 359-bp sequence of the 1.688 satellite DNA, repeats of which comprise approximately 11 Mb of the heterochromatin proximal to the *X* chromosome centromere (Dernburg *et al.* 1996). Females of each genotype were fattened for 1–2 days on yeast with males. Ovaries from 12 females were dissected in 1× modified Robb's solution (Theurkauf and Hawley 1992), gently splayed open with a tungsten needle, and transferred to a microfuge tube. Preheated (37°) fix solution (4% formaldehyde, 0.1 M sodium cacodylate, 0.1 M sucrose, 0.04 M sodium acetate, and 0.01 M EGTA) was added to the ovaries, the tube was nutated for 3 min at room temperature, and the ovaries were allowed to settle for 1 min. Ovaries were rinsed three times and washed three times for 10 min in 2× SSCT (0.3 M sodium chloride, 0.03 M sodium citrate, and 0.1% Tween-20) and then incubated for 10 min each in 20, 40, and 50% formamide in 2× SSCT at room temperature. Samples were incubated for 2 hr at 37° in prewarmed 50% formamide in 2× SSCT and then transferred to a 0.2-ml PCR tube. Then 40 μl of hybridization buffer (3× SSC, 50% formamide, 10% dextran sulfate, and 2.5 ng/μl 359 probe) was added, and the samples were incubated in a PCR machine at 37° for 5 min, 92° for 3 min, and 37° overnight. Following hybridization, ovaries were transferred to a 0.5-ml microfuge tube and washed three times for 20 min and three times for 10 min at 37° in prewarmed 50% formamide in 2× SSCT, moved to room temperature, and washed for 10 min each in 50, 40, and 20% formamide in 2× SSCT and for 10 min in 2× SSCT. A 20-min incubation in DAPI (1.0 μg/ml in 2× SSCT) was followed by three rinses and two times 10-min washes in 2× SSCT. Stained ovaries were separated into individual ovarioles with tungsten needles, spread on

poly-L-lysine-coated coverslips, and mounted in Prolong Gold (Molecular Probes).

FISH scoring

Each slide was scanned systematically, and ovarioles were scored as they were encountered. Ovarioles were scored only if they contained four or more egg chambers with clearly discernible oocyte nuclei. The developmental stage of each egg chamber was determined based on size and morphology (Ashburner *et al.* 2005). The "two-spot" phenotype was assigned to oocytes in which the DAPI signal colocalized with two distinct FISH spots and in which a small spot was clearly visible, distinct from the larger spot, and in which the two spots were separated by at least the diameter of the small spot. In addition to the phenotypes depicted in Figure 1C, other configurations were observed occasionally. Two spots of equal size were interpreted as representing the satellite region of the normal *X* chromosome and the distal end of *FM7a*, with the small *FM7a* pericentric region associated with one or the other. Because we could not be certain in this case whether the pericentric regions were associated or apart, these oocytes were conservatively scored as exhibiting "normal" PHeMAAH. When two large spots and a single small spot were observed, this was interpreted as indicating separation of all three regions of satellite sequence and scored as "defective" PHeMAAH because the pericentric regions of the two chromosomes were unambiguously separated. KD and control genotypes were compared using a two-tailed Fisher's exact test to obtain *P*-values. Thirty ovarioles were scored per slide. For each genotype, because we observed negligible variation between slides, we pooled our results when more than one slide was scored. Then 95% confidence intervals were calculated using the modified Wald method (Agresti and Coull 1998) available on GraphPad.

Chromosome spreads

Preparation of chromosome spreads was performed as described previously (Khetani and Bickel 2007), with the exception that incubation in primary antibodies extended overnight, and slides were mounted in Prolong Gold (Molecular Probes). Primary antibodies and dilutions used were chicken α-CID at 1:250 (Blower and Karpen 2001), mouse α-C(3)G at 1:2000 (Page and Hawley 2001), and rabbit α-Piwi at 1:1000 (Klattenhoff *et al.* 2009). Secondary antibodies, all used at a final dilution of 1:400, were Alexa 488–conjugated donkey α-mouse (Invitrogen) and Cy3-conjugated donkey α-rabbit and Cy5-conjugated donkey α-chicken (both from Jackson Immunoresearch Laboratories).

Visualization of ovary GFP-HP1a expression

Ovaries from eight or nine fattened females were dissected in 1× PBS, fixed in 4% formaldehyde in 1× PBS for 5 min, and rinsed three times in 1× PBS. Samples were incubated for 30 min in 2.0 μg/ml Hoechst 33342 in 1× PBS in the dark and then rinsed and washed in 1× PBS. Individual ovarioles were separated and mounted on poly-L-lysine-coated coverslips in Prolong Diamond (Molecular Probes).

Microscopy, imaging, and image processing

FISH analysis was performed using a 1.4-NA 100× Plan APOCHROMAT Objective on a Zeiss Axioimager M1 Microscope with a Hamamatsu C10600-10B Orca-R2 camera controlled by Volocity 6.3 software (Perkin-Elmer). FISH spots were analyzed by focusing up and down and while viewing an enlarged image on the computer screen. Images of FISH spots and chromosome spreads were captured using a 1.4-NA 63× Plan APOCHROMAT Objective on the same microscope and represent maximum-intensity projections of Z series (0.1-μm steps) that were deconvolved using Volocity 6.3 (20 iterations) and then cropped in the Z to 0.7 μm (spreads) or 0.5 μm (FISH). For chromosome spreads, Cy3 (Piwi) images corresponding to "plus" or "minus" Piwi primary antibody were acquired, processed, and contrast enhanced identically. However, different settings were used for 16-cell cysts and individual nuclei. Images of GFP-HP1a expression in ovaries were acquired using a 40× Oil Plan Fluor DIC objective (NA 1.3) on a Nikon A1RSi Laser Scanning Confocal Microscope controlled by NIS Elements software v4.30.02. Single optical sections were captured using 407- (DAPI) and 488-nm (GFP) lasers. Ovariole images were captured without digital zoom, while magnified images of oocyte nuclei were captured using 4× digital zoom; otherwise, all images were captured and processed identically.

Quantification of ovary GFP-HP1a expression

Confocal images of ovarioles expressing the UAS-driven wild-type or W200A GFP-HP1a transgene were used to quantify GFP-HP1a expression and compare relative expression levels at different stages of oogenesis. For each genotype, three representative ovarioles were selected, and egg chambers were assigned a developmental stage based on size and morphology. Within each egg chamber, three nurse cell nuclei with clearly defined boundaries were selected. The GFP signal within each nucleus was quantified using Volocity 6.3 software, and the mean GFP nuclear intensity was calculated for that egg chamber. For each developmental stage, the average nuclear GFP signal intensity for three egg chambers was graphed. An unpaired *t*-test was used to compare the nuclear GFP intensity from the three wild-type GFP-HP1a and three W200A GFP-HP1a egg chambers for each stage.

Data availability

The authors state that all data necessary for confirming the conclusions presented in this article are represented fully within the article. Constructs and strains are available on request.

Results

Reducing HP1a levels causes FM7a/X segregation errors in oocytes

Drosophila FM7a/X females are a useful model system for studying the association and segregation of achiasmate chromosomes. The *FM7a* balancer is a derivative of the *X*

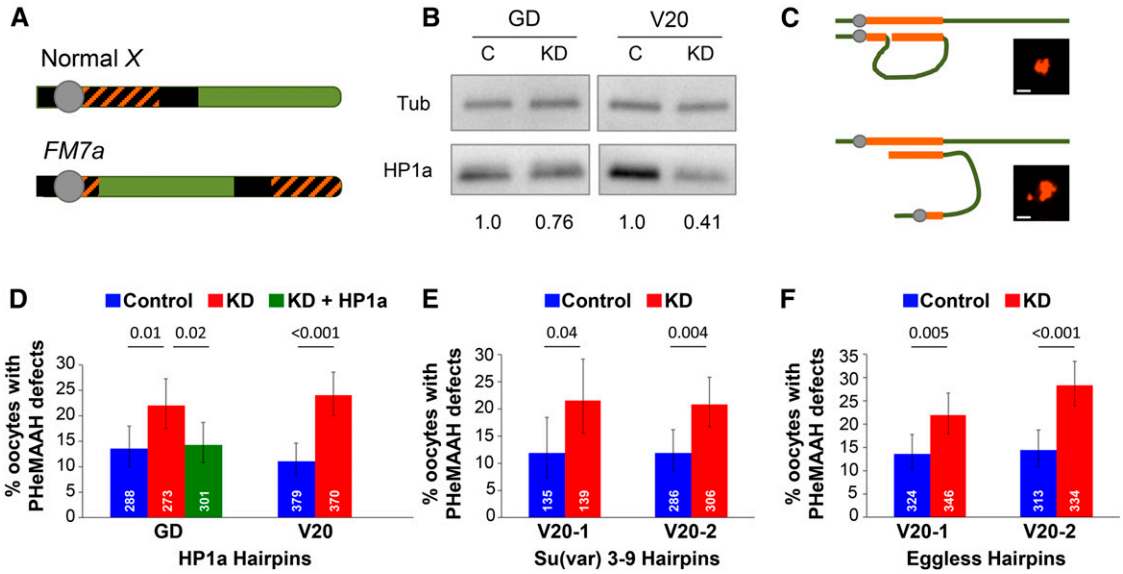

Figure 1 Reduction of HP1a protein or H3K9 methyltransferases in *FM7a/X* oocytes disrupts PHeMAAH. (A) Diagram of wild-type *Drosophila X* chromosome and its derivative, the *FM7a* balancer. Heterochromatin is shown as black. Orange cross-hatching denotes the 359-bp satellite DNA repeats recognized by the FISH probe. The centromere is the gray circle. Rearrangements within the *FM7a* euchromatin (green) suppress recombination with a normal *X* chromosome. (B) Immunoblots of ovary extracts from HP1a knockdown (KD) and control (C) flies. The relative intensity of HP1a signal for each set of knockdown and control extracts is shown below the blot. For each lane, HP1a signals were normalized to tubulin. GD and V20 correspond to the HP1a hairpins used for knockdown. (C) Schematic diagram of heterochromatic pairing between *FM7a* and a normal *X* chromosome. Pairing between euchromatic regions has been omitted for clarity. The 359-bp repeats are shown in orange. When PHeMAAH is normal (top), association between heterochromatic regions results in one large, visible FISH signal. When PHeMAAH is disrupted (bottom), the pericentric regions separate, resulting in one small dot corresponding to the *FM7a* pericentric region and one large dot representing the remaining 359-bp repeats of the *FM7a* and normal *X* chromosomes. Inset images show representative oocyte FISH signals. Scale bars, 1.0 μm. See *Materials and Methods* for other heterochromatin pairing configurations not shown. (D–F) Levels of *FM7a/X* PHeMAAH defects measured by FISH. *P*-values are shown above the bars, and 95% confidence intervals are presented as error bars. Number of oocytes assayed for each genotype is indicated in white. Control flies carry the UAS hairpin transgene but lack the matα driver, so the hairpin is not expressed. KD flies express the hairpin under the control of the matα driver (see *Materials and Methods*). Complete data for these experiments are provided in Table S3. (D) In HP1a RNAi experiments, 60 ovarioles were scored for each genotype using the GD hairpin, and 90 ovarioles were scored for each V20 hairpin genotype. (E) In Su(var)3–9 RNAi experiments, 30 and 60 ovarioles were scored for each genotype containing the V20-1 and V20-2 hairpins, respectively. (F) For both Eggless hairpins, 60 ovarioles were scored for each genotype.

chromosome for which much of the pericentric heterochromatin has been translocated to the distal end of the arm (Figure 1A). The euchromatin of *FM7a* also contains several inversions that suppress recombination with a normal *X* even though pairing and synapsis occur normally in the majority of *FM7a/X* oocytes (Hawley *et al.* 1993; Gong *et al.* 2005). Therefore, *FM7a/X* homologs rely entirely on the achiasmate system for accurate segregation. We have previously shown that because centromere proximal heterochromatin on *FM7a* is greatly reduced, the *FM7a/X* pair provides a sensitized system to investigate the mechanisms underlying PHeMAAH (Subramanian and Bickel 2009).

We predicted that reducing the amount of any protein required for PHeMAAH would lead to weakened *FM7a/X* association, which should, in turn, cause an increase in *X* chromosome segregation errors. Therefore, to begin to investigate the role of HP1a in achiasmate homolog association, we measured *X* chromosome NDJ during meiosis in *FM7a/X* females that also were heterozygous for the *Su(var)205*^{5} null allele (Eissenberg *et al.* 1992). In a genetic test that provides a quantitative measure of the fidelity of chromosome segregation during meiosis (Figure S1), we observed a small but statistically significant increase in *FM7a/X* chromosome NDJ in *Su(var)205*^{5} heterozygotes compared to control *FM7a/X* flies lacking the mutation (1.69% in mutant *vs.* 0.49% in control, $P < 0.0001$; Table 1). This result suggests that the heterochromatin protein HP1a promotes accurate segregation of achiasmate homologs in *Drosophila* oocytes.

Because HP1a is an essential gene product, we cannot assay for meiotic chromosome segregation defects in homozygotes (which are nonviable), and heterozygotes have reduced levels of HP1a in all somatic cells as well as in the germline. In order to focus more narrowly on the role of HP1a in oocytes, we turned to a UAS/Gal4-inducible RNAi strategy. We used the female germline-specific driver matα Gal4:VP16 (matα driver) (Januschke *et al.* 2002), which is first expressed in region three of the germarium and remains active as oogenesis progresses (Weng *et al.* 2014). The matα driver allowed us to induce expression of an HP1a RNAi hairpin starting in mid-prophase, well after homologs synapse and meiotic recombination begins. Therefore, this approach allowed us to specifically ask whether normal levels of HP1a in the oocyte

Table 1 Reduction of HP1a induces increased *FM7A/X* nondisjunction

Genotype	% NDJ	% Diplo (*n*)	% Nullo (*n*)	Total *n*	*P*-value
FM7a/y; Su(var)205^5/+	1.69%	0.83% (23)	0.86% (24)	5513	<0.0001
FM7a/y; cn bw sp/+	0.49%	0.27% (5)	0.22% (4)	3680	
FM7a/y w; HP1a RNAi^{GD}/+; matα/+	1.69%	0.92% (12)	0.77% (10)	2610	0.001
FM7a/y w; HP1a RNAi^{GD}/+; +/+	0.33%	0.25% (3)	0.08% (1)	2399	

are required to maintain pericentric association and for proper segregation of achiasmate homologs. For all the RNAi experiments we describe, "knockdown" (KD) refers to flies that express an RNAi hairpin driven by the matα driver, while "control" refers to flies that carry the RNAi transgene but lack the driver and therefore do not express the hairpin. We measured meiotic NDJ in *FM7a/X* flies expressing the HP1a RNAi^{GD} hairpin (Figure S2) in the germline and observed a result very similar to that seen in *Su(var)205^5* heterozygotes: knockdown of HP1a caused a small but statistically significant increase in *X* chromosome NDJ during meiosis (1.69% in KD *vs.* 0.33% in control, $P = 0.001$; Table 1). Immunoblotting confirmed that matα-driven expression of the HP1a RNAi^{GD} hairpin reduced HP1a protein in the ovary (Figure 1B) to a level that was comparable to that observed in Su(var)205^5 heterozygotes (Figure S3). Our finding that reduction of HP1a by two different methods causes similar levels of achiasmate homolog missegregation confirms that the NDJ phenotype we observe is not an artifact of genetic background. We conclude that reduced levels of HP1a protein in the oocyte compromises segregation of the achiasmate *FM7a/X* chromosome pair.

Knockdown of HP1a in oocytes weakens pericentric heterochromatin-mediated association of achiasmate homologs

Because accurate segregation of achiasmate homologs depends on their stable association during meiotic prophase, our finding that HP1a knockdown in oocytes causes chromosome segregation errors suggests that the physical association of achiasmate homologs may be disrupted when HP1a levels are reduced. To directly visualize PHeMAAH in *FM7a/X* oocytes, we performed FISH using a probe that hybridizes to the 359-bp satellite repeat sequence that comprises a large percentage of the heterochromatin on the *X* chromosome (Hsieh and Brutlag 1979) (Figure 1A). As illustrated in Figure 1C, one FISH signal within the oocyte nucleus indicates that the centromere proximal heterochromatin of *FM7a* is physically associated with that of the normal *X* chromosome, and this represents "normal" PHeMAAH (Dernburg *et al.* 1996). However, defects in PHeMAAH are manifest as visible separation of the small region of pericentric heterochromatin on *FM7a* (small dot) from the large heterochromatin signal corresponding to the normal *X* chromosome and distal heterochromatin on *FM7a* (large dot) (Figure 1C). We used the presence of a small FISH dot in combination with one or two large FISH signals to quantify the number of *FM7a/X* oocytes exhibiting "defective" PHeMAAH.

When we probed ovaries from *FM7a/X* females expressing the HP1a RNAi^{GD} hairpin, we observed a significant increase in PHeMAAH defects in KD oocytes compared to control (22.0% in KD *vs.* 13.5% in the control, $P = 0.01$), indicating that the pericentric heterochomatin-mediated association of *FM7a* and a normal *X* chromosome was weaker and/or disrupted in HP1a KD oocytes (Figure 1D). We also obtained a very similar result (24.0% in KD *vs.* 11.1% in control, $P < 0.001$; Figure 1D) when using the HP1a RNAi^{V20} hairpin, which targets a different region of the HP1a mRNA (Figure S2). Because two different hairpins that reduce HP1a protein levels in ovaries (Figure 1B) both result in disruption of PHeMAAH, we can conclude that the defects that we observe are not the result of RNAi off-target effects. Interestingly, when we pooled data from multiple experiments and tabulated FISH results for different stages of oogenesis (Figure S4 and Table S4), we found that PHeMAAH defects were significantly increased in HP1a KD oocytes primarily during middle to late oogenesis (stages 7–10), after disassembly of the synaptonemal complex. However, knockdown of HP1a also caused a significant increase in PHeMAAH defects at earlier stages (stages 2–3) when the synaptonemal complex is still intact.

We reasoned that if the PHeMAAH defects we observe in *FM7a/X* HP1a KD oocytes are due solely to reduction of HP1a protein, increasing HP1a levels in HP1a KD oocytes should rescue the phenotype. To test this hypothesis, we used the matα driver to induce germline expression of the HP1a RNAi^{GD} transgene in *FM7a/X* females that also harbored one copy of a GFP-HP1a transgene containing *Su(var)205* regulatory sequences that control its expression (Wen *et al.* 2008; Lipsick 2010). When we performed FISH, the number of oocytes exhibiting PHeMAAH defects was significantly lower ($P = 0.02$) for HP1a RNAi^{GD} KD oocytes expressing the GFP-HP1a transgene (14.3%) than for HP1a RNAi^{GD} KD oocytes that lacked the GFP-HP1a transgene (22.0%) (Figure 1D). Notably, expression of GFP-HP1a resulted in pericentric heterochromatin-mediated association between *FM7a* and a normal *X* chromosome that was comparable to that observed in control oocytes ($P = 0.91$) (Figure 1D). Together these data support the conclusion that reduction of HP1a levels in the oocyte leads to weakening and/or loss of pericentric heterochromatin-mediated association of achiasmate chromosomes.

Knockdown of two different H3K9 methyltransferases disrupts PHeMAAH

Because PHeMAAH specifically depends on pericentric heterochromatin, and because proper localization of HP1a to

pericentric heterochromatin depends on deposition of the H3K9me2/3 mark by the methyltransferase Su(var)3–9 (Schotta *et al.* 2002), we asked whether PHeMAAH is affected by reduction of Su(var)3–9 in the oocyte. Using two different RNAi hairpins that target different regions of the mRNA (Figure S2), we knocked down Su(var)3–9 in *FM7a/X* oocytes and assayed for PHeMAAH defects using FISH. With both hairpins, we observed that Su(var)3–9 knockdown induced defects at levels similar to those in HP1a knockdown oocytes (V20-1: 21.6% in KD *vs.* 12.4% in control, $P = 0.04$; V20-2: 20.9% in KD *vs.* 11.9% in control, $P = 0.004$; Figure 1E). These results are consistent with the hypothesis that proper localization of HP1a to pericentric heterochromatin is required to support PHeMAAH.

Interpretation of the Su(var)3–9 result is somewhat complicated by the fact that owing to a quirk of *Drosophila* evolutionary history, the *Su(var)3–9* gene shares an exon with that of the translation initiation factor *eIF-γ* (Krauss and Reuter 2000). Unfortunately, all publically available Su(var)3–9 hairpins target sequences in this common exon, raising the possibility that the PHeMAAH defects that we observe in Su(var)3–9 KD oocytes result from disruption of *eIF-γ* function rather than reduced H3K9 methyltransferase activity. To further investigate the requirement of the H3K9me2/3 mark for promoting centromere proximal association of achiasmate homologs, we knocked down Eggless (also known as dSETDB1), a second methyltransferase that is also required to maintain the H3K9me2/3 mark in the pericentric heterochromatin (Brower-Toland *et al.* 2009). With two different hairpins targeting different sequences within the Eggless mRNA (Figure S2), *FM7a/X* KD oocytes exhibited a significant increase in PHeMAAH defects compared to control oocytes (V20-1: 22.0% in KD *vs.* 13.6% in control, $P = 0.005$; V20-2: 28.4% in KD *vs.* 14.4% in control, $P < 0.001$; Figure 1F). Although we cannot rule out the possibility that knockdown of *eIF-γ* may contribute to PHeMAAH defects, the striking similarity in the results we observe for Su(var)3–9 and Eggless KD argues that maintenance of the H3K9 methyl mark and recruitment of HP1a to pericentric heterochromatin are required to promote the centromere proximal association of achiasmate homologs in *Drosophila* oocytes.

Given that the knockdown of HP1a, Su(var)3–9, and Eggless all result in a similar elevation of PHeMAAH defects compared to control oocytes, we performed an additional control to rule out the possibility that matα-driven expression of any RNAi hairpin in the oocyte will cause disruption of PHeMAAH. For this experiment, we used the matα driver to induce expression of a GFP RNAi hairpin in *FM7a/X* females that lacked a GFP target (no transgene encoding GFP or a GFP fusion protein). Expression of the GFP RNAi hairpin did not cause a significant increase in PHeMAAH defects compared to control oocytes lacking the driver (16.6% in KD *vs.* 13.3% in control, $P = 0.4$), demonstrating that matα-driven hairpin expression alone does not cause weakening of centromere proximal heterochromatin-mediated pairing of the *FM7a/X* homologs (Figure S5).

Piwi protein stably associates with oocyte chromosomes

A member of the Argonaute protein family, Piwi is able to bind piRNAs and repress the mobilization of retrotransposons within the germline (Mani and Juliano 2013; Ku and Lin 2014). However, Piwi is also a recognized binding partner of HP1a (Brower-Toland *et al.* 2007), plays a role in the establishment of heterochromatin during early embryogenesis (Gu and Elgin 2013), and is required for pairing-sensitive silencing (Grimaud *et al.* 2006), a phenomenon that involves crosstalk between homologous chromosomes (Kassis 1994; Americo *et al.* 2002). Therefore, we set out to test the hypothesis that Piwi, possibly in collaboration with HP1a, promotes the pericentric heterochromatin-mediated association of achiasmate homologs that is required for their accurate segregation in the *Drosophila* oocyte.

Localization of Piwi within the nuclei of nurse cells and the oocyte has been well established using whole-mount ovary preparations (Brennecke *et al.* 2007; Klattenhoff *et al.* 2009; Wang and Elgin 2011; Darricarrère *et al.* 2013; Dufourt *et al.* 2014); however, these data have not yielded conclusive evidence that Piwi physically associates with oocyte chromatin. Therefore, we used ovaries from wild-type females to prepare chromosome spreads, a technique in which cytosolic proteins are removed as well as nuclear proteins that are not bound to chromatin (Peters *et al.* 1997; Khetani and Bickel 2007). This approach, coupled with standard immunostaining, facilitates visualization of proteins that are stably associated with the oocyte chromosomes (Webber *et al.* 2004; Khetani and Bickel 2007; Page *et al.* 2008). We used the synaptonemal complex protein C(3)G (Page and Hawley 2001) as a marker to identify oocyte chromosomes and the centromere-specific histone variant CID (Blower and Karpen 2001) to mark the centromeres. Using antiserum specific for Piwi (Klattenhoff *et al.* 2009), we observed binding of Piwi protein to multiple sites along the meiotic chromosomes. In some cases, the spread chromosomes from all 16 nuclei of a germarial cyst remain in close proximity on the slide (Figure 2A). Note that Piwi is localized to the chromatin of all 16 nuclei and that the signal intensity in the two pro-oocytes [long C(3)G threads] is similar to that of the adjacent pro-nurse cells. Interestingly, Piwi binding to the chromatin does not appear uniform; instead, numerous patches of enrichment are visible, contrasting sharply with the homogeneous signal we have reported for spread preparations stained with histone antibodies (Khetani and Bickel 2007). This nonuniform Piwi staining pattern is especially apparent in Figure 2B, which shows an isolated spread from a pachytene oocyte, most likely at a later stage of oogenesis. Regions of Piwi enrichment often lie adjacent to the C(3)G threads but do not colocalize extensively with the synaptonemal complex. Moreover, Piwi signal is not restricted to the pericentric heterochromatin, but it is clearly visible in the vicinity of the centromeres. Because *piwi* mutations disrupt germline stem cell maintenance, we could not prepare spreads from ovaries lacking Piwi protein. However, Figure 2, C and D, shows negative controls in which spread

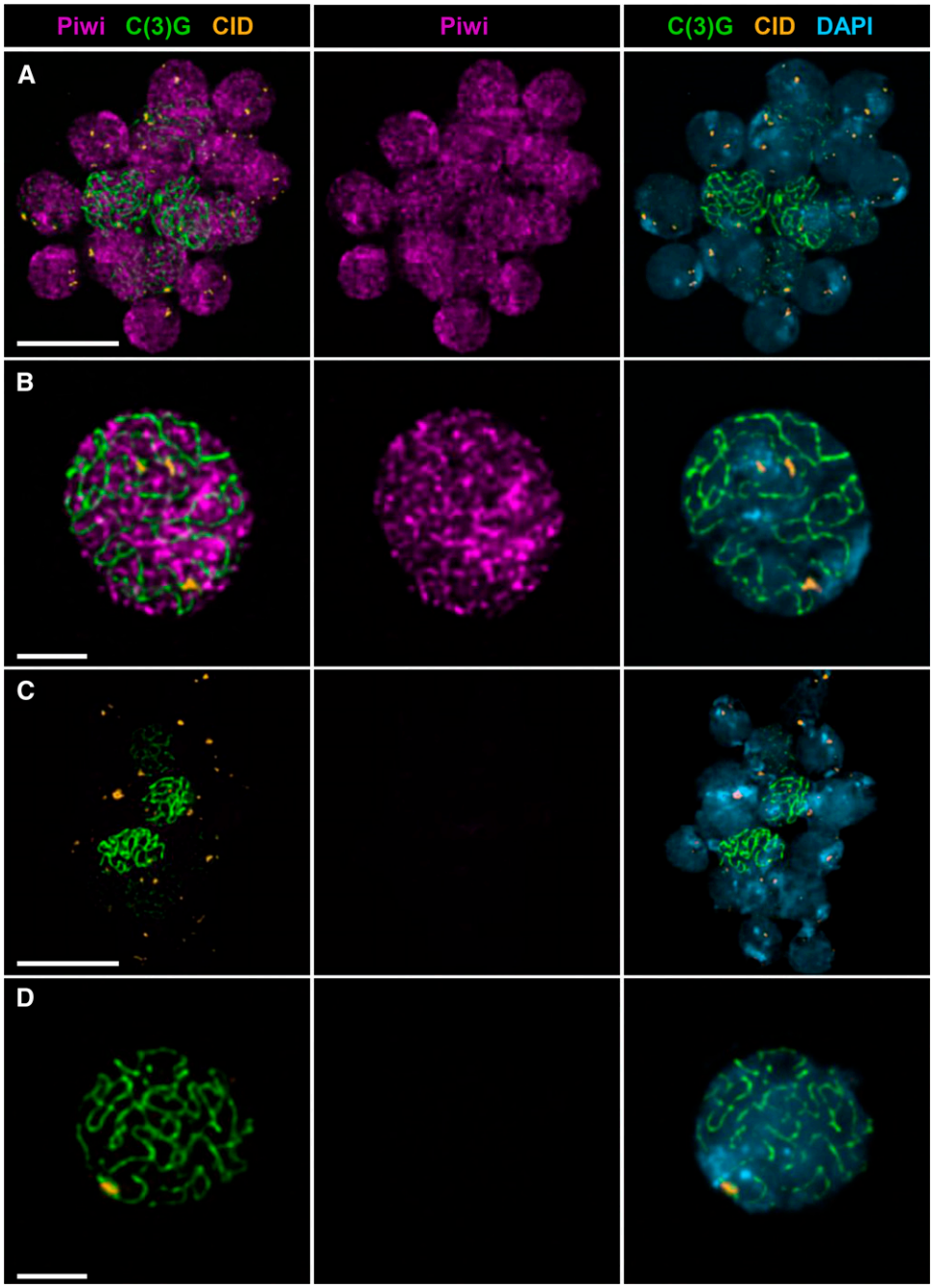

Figure 2 Piwi localizes to oocyte chromatin throughout the genome. Chromosome spread preparations from wild-type ovaries were stained with antibodies that recognize Piwi (magenta), the synaptonemal complex protein C(3)G (green), and the centromere marker CID (orange) and counterstained with DAPI (blue). Images are maximum-intensity projections of a deconvolved Z series (see *Materials and Methods*). (A) Chromatin from 16 interconnected cells of an early meiotic cyst. C(3)G staining indicates that full-length synaptonemal complex is present in two adjacent cells, corresponding to region 2B of the germarium. Piwi localizes to the chromatin in a nonuniform pattern in both pro-oocytes and pro-nurse cells. (B) Chromosome spread from a single pachytene nucleus, most likely from a postgermarial egg chamber. Piwi localizes to discrete regions along the meiotic chromosomes. Regions of Piwi enrichment are visible, including heterochromatin near the centromeres (marked with CID). (C and D) Chromatin from semi-intact 16-cell cyst (C) and single nucleus (D) stained for C(3)G and CID and counterstained with DAPI. Primary antibody against Piwi was omitted, but secondary antibody was included. Piwi images were captured and processed identically for A and C and for B and D pairs. Scale bars correspond to 10 μm in A and C and 3 μm in B and D.

preparations were stained identically except that the Piwi antibody was omitted. From these experiments, we conclude that Piwi is able to associate with the oocyte chromosomes and that its localization within pericentric heterochromatin is consistent with a possible role in PHeMAAH.

Reduction of Piwi during mid-prophase causes PHeMAAH defects and missegregation of achiasmate homologs

If Piwi promotes the centromere proximal association of the *FM7a/X* homologs, then reduction of Piwi levels by RNAi may affect their segregation. Immunoblotting confirmed that matα-driven RNAi knockdown of Piwi lowered Piwi protein levels in ovary extracts (Figure 3A). Although induction of Piwi knockdown with the matα driver does not begin until mid-prophase, fertility of Piwi KD females was still strongly reduced. However, we were able to recover sufficient progeny from *FM7a/X* females expressing the Piwi RNAi$^{V20\text{-}1}$ hairpin (Figure S2) to measure meiotic NDJ levels (Table 2). We observed a significant increase in *FM7a/X* NDJ in Piwi KD oocytes compared to control oocytes (16.4% NDJ in KD *vs.* 1.4% in control, $P = 0.004$), indicating that normal levels of Piwi are required for the accurate segregation of achiasmate chromosomes.

If chromosome segregation errors arise in Piwi KD oocytes because Piwi is required to promote pericentric heterochromatin-mediated association of achiasmate

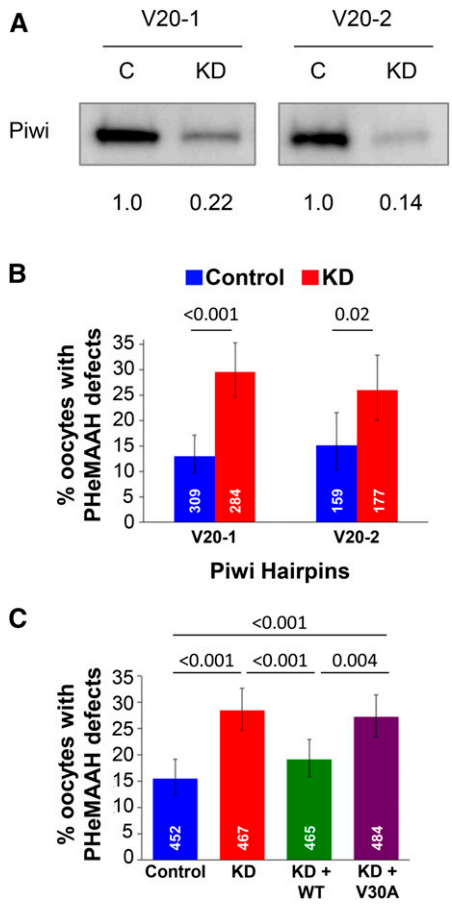

Figure 3 Knockdown of Piwi in the germline causes PHeMAAH defects, which can be rescued by wild-type, but not mutant, Piwi expression. (A) Western blot comparing Piwi levels in knockdown (KD) and control (C) ovary extracts from flies harboring the Piwi V20-1 or the V20-2 hairpin. For each lane, the Piwi signal intensity was normalized to the total protein in the corresponding lane of the blot, and the relative levels of Piwi protein in knockdown and control extracts are shown below the blots. (B) Matα-driven expression of two hairpins targeting different regions of the Piwi mRNA both result in PHeMAAH defects for *FM7a/X* chromosomes. Sixty ovarioles per genotype were scored for the V20-1 hairpin, and 30 ovarioles were scored for each V20-2 genotype. (C) *FM7a/X* PHeMAAH defects caused by Piwi knockdown can be rescued by expression of a wild-type (WT) Piwi transgene but not a transgene encoding the V30A Piwi mutant protein. "Control" oocytes carry the Piwi RNAi$^{V20\text{-}1}$ hairpin transgene but lack the Gal4 driver, so the hairpin is not expressed. "KD" oocytes express the RNAi$^{V20\text{-}1}$ hairpin under control of the matα driver. "KD + WT" oocytes express the Piwi UAS-RNAi$^{V20\text{-}1}$ hairpin and also contain a wild-type Piwi transgene in which Piwi expression is controlled by native Piwi regulatory sequences. "KD + V30A" oocytes express the RNAi$^{V20\text{-}1}$ Piwi hairpin and also harbor a transgene in which native Piwi regulatory sequences control expression of Piwi protein containing a V30A mutation. Ninety ovarioles of each genotype were scored. For B and C, the number of individual oocytes scored for each genotype is indicated in white, and *P*-values are shown above the bars. Error bars represent 95% confidence intervals. Complete data for FISH experiments are provided in Table S3.

homologs, we reasoned that a significant increase in PHeMAAH defects should be evident in *FM7a/X* Piwi KD oocytes analyzed by FISH. Using two independent Piwi hairpins (denoted V20-1 and V20-2; Figure S2) that both reduce Piwi protein levels in the ovary (Figure 3A), we observed a significantly higher percentage of PHeMAAH defects in KD oocytes than in control oocytes (V20-1: 29.6% in KD *vs.* 12.9% in control, $P < 0.001$; V20-2: 26.0% in KD *vs.* 15.1% in control, $P = 0.02$; Figure 3B). In addition, when we analyzed FISH data from multiple experiments and quantified PHeMAAH defects at different oocyte stages, we found that the temporal profile for Piwi KD-induced defects was strikingly similar to what we observed for HP1a KD oocytes (Figure S4 and Table S4). Notably, it was during middle to late oogenesis that the most dramatic differences were observed between Piwi KD and control oocytes, specifically the stages that follow disassembly of the synaptonemal complex. However, like HP1a KD, knockdown of Piwi caused a significant increase in PHeMAAH defects as oocytes exited the germarium (stage 2). These data, combined with the published evidence that HP1a and Piwi physically interact (Brower-Toland *et al.* 2007), suggest that the two proteins may indeed be collaborating to promote the association and segregation of achiasmate homologs in *Drosophila* oocytes.

Wild-type Piwi protein but not the V30A Piwi mutant protein promotes PHeMAAH

In order to demonstrate that the elevation of PHeMAAH defects we observed in Piwi KD oocytes is genuinely due to reduced levels of Piwi protein, we performed a rescue experiment similar to that described earlier for HP1a. For this experiment, we used a Piwi transgene in which the native Piwi promoter controls expression of wild-type Piwi protein (Brower-Toland *et al.* 2007). For *FM7a/X* flies that expressed both the Piwi RNAi$^{V20\text{-}1}$ hairpin and a single copy of the wild-type Piwi transgene (KD + WT, Figure 3C), PHeMAAH defects were significantly lower than for Piwi RNAi$^{V20\text{-}1}$ KD oocytes that lacked the Piwi transgene (19.1% in KD + WT *vs.* 28.5% in KD, $P < 0.001$) and not significantly different from control females that contained the Piwi RNAi$^{V20\text{-}1}$ hairpin but no matα driver (15.5% in control; for control *vs.* KD + WT, $P = 0.16$; Figure 3C). We also tested an additional Piwi transgene encoding a mutant version of Piwi protein (V30A) that is unable to interact with HP1a (Brower-Toland *et al.* 2007). Unlike the wild-type Piwi transgene, V30A Piwi failed to rescue the PHeMAAH defects caused by expression of the Piwi RNAi$^{V20\text{-}1}$ hairpin in *FM7a/X* oocytes (27.3% in KD + V30A *vs.* 28.5% in KD, $P = 0.7$; *vs.* 15.5% in control, $P < 0.001$; Figure 3C). We verified that Piwi protein levels were increased in both KD + WT and KD + V30A extracts relative to KD only (Figure S6). From these data, we conclude that Piwi is required for accurate chromosome segregation of achiasmate homologs because it helps to promote their pericentric heterochromatin-mediated association during prophase I. Importantly, our finding that the V30A point mutation in the Piwi transgene abolishes its ability to rescue PHeMAAH defects in Piwi KD oocytes supports the model that centromere proximal association of achiasmate chromosomes in *Drosophila* oocytes requires physical interaction of Piwi with the HP1a protein.

Table 2 Piwi RNAi KD increases nondisjunction of *FM7A/X* chromosomes

Genotype	% NDJ	% Diplo (*n*)	% Nullo (*n*)	Total *n*	*P*-value
w B/FM7a;+;Piwi RNAi$^{V20\text{-}1}$/matα	16.39%	9.84% (6)	6.56% (4)	122	0.004
w B/FM7a:+;Piwi RNAi$^{V20\text{-}1}$/+	1.44%	1.03% (5)	0.41% (2)	969	

Mutant HP1a protein that is unable to bind Piwi fails to promote PHeMAAH

We used an alternative approach to confirm that interaction of Piwi with HP1a is required for pericentric heterochromatin-mediated association of achiasmate homologs. The W200A mutation in HP1a lies within the CSD and has been shown to abolish the ability of HP1a to interact with Piwi (Brower-Toland *et al.* 2007; Mendez *et al.* 2011). W200A HP1a dimers still form, but the binding surface formed by HP1a dimerization does not support association with Piwi (Brower-Toland *et al.* 2007; Mendez *et al.* 2011). Therefore, we generated UAS/Gal4-inducible transgenes that encoded either wild-type or W200A mutant HP1a tagged with GFP (Figure 4A). Both transgenes lack the 3′ UTR region of the endogenous HP1a mRNA and are therefore resistant to the HP1a RNAi^{V20} hairpin (Figure S2). In *FM7a/X* oocytes in which the matα driver simultaneously induced expression of both the wild-type GFP-HP1a transgene and the HP1a RNAi^{V20} hairpin (KD + WT), PHeMAAH defects were significantly lower than in KD oocytes expressing only the HP1a RNAi^{V20} hairpin (KD + WT: 17.7%, KD: 25.4%, $P = 0.02$; Figure 4B).

Importantly, expression of the wild-type GFP-HP1a transgene in HP1a KD oocytes (KD + WT) resulted in PHeMAAH defects that were comparable to control oocytes harboring both HP1a transgenes but lacking the matα driver (KD + WT: 17.7%, control: 16.9%, $P = 0.84$; Figure 4B). These data indicate that matα-driven expression of our UAS/Gal4-inducible wild-type GFP-HP1a construct can rescue the KD phenotype. In contrast, simultaneous expression of the W200A GFP-HP1a transgene with the HP1a RNAi^{V20} hairpin in *FM7a/X* oocytes fails to rescue PHeMAAH defects caused by HP1a KD (KD + W200A: 26.3%; $P = 0.80$ when compared to KD alone and $P = 0.003$ when compared to control; Figure 4B). Therefore, results from two independent experimental approaches (Figure 3C and Figure 4B) support the hypothesis that physical interaction of HP1a with Piwi is required to maintain the pericentric heterochromatin-mediated association of achiasmate homologs during meiotic prophase.

We performed an additional control to verify that the lack of rescue observed with the W200A mutant HP1a protein was not due to low expression or mislocalization. Using confocal imaging, we compared GFP-HP1a signal intensity and localization in the ovarioles of three genotypes: females with matα-driven expression of wild-type GFP-HP1a and HP1a RNAi^{V20} (WT), females in which matα is driving expression of the W200A GFP-HP1a transgene and the HP1a RNAi^{V20} hairpin (W200A), and females that harbored both the WT GFP-HP1a and the HP1a RNAi^{V20} transgenes but lacked a driver (no GFP-HP1a expression). Figure 5 shows representative ovariole images that were captured and processed identically for each genotype. The GFP fluorescence intensity is comparable for WT GFP-HP1a and W200A GFP-HP1a ovarioles, and both WT and W200A GFP HP1a proteins localize to the nurse cell and oocyte nuclei (compare Figure 5, A and F). No nuclear GFP signal is detectable in the control ovarioles (no GFP-HP1) (Figure 5K). In nurse cell nuclei, bright foci for both WT and W200A GFP-HP1a are visible and most likely correspond to HP1a association with specific genomic regions. In the oocyte nuclei, bright regions of GFP-HP1a signal are restricted to the area occupied by the karyosome (oocyte DNA), indicating that both WT and W200A GFP-HP1a can localize to the oocyte chromosomes (Figure 5, C–E and H–J). Quantification of GFP-HP1a signal intensity in nurse cell nuclei at different stages of oogenesis confirms that the level of nuclear W200A is comparable or slightly higher than that of WT GFP-HP1a (Figure 5P). Therefore, failure of W200A GFP-HP1a to rescue the PHeMAAH defects caused by HP1a KD cannot be explained by poor expression or mislocalization of the mutant protein.

We also carried out an additional set of experiments to rule out the possibility that titration of the Gal4:VP16 produced by the matα driver was limiting in the presence of two UAS-controlled transgenes (Figure S7). If this were the case, a reduction of HP1a KD PHeMAAH defects could arise when the UAS/Gal4-inducible WT GFP-HP1a transgene is present not because of "true rescue" but because expression of the UAS-RNAi hairpin is lower in the presence of another UAS transgene. However, when we measured PHeMAAH defects in *FM7a/X* females that harbored the UAS-HP1a RNAi^{V20} hairpin as well as a UAS-GFP RNAi hairpin (but no transgene encoding a GFP protein), we found that the levels of PHeMAAH defects were comparable to those observed when matα was driving only the single UAS-HP1a RNAi^{V20} hairpin (Figure S7; compare HP1a KD with HP1a KD + GFP RNAi, $P = 0.86$). Therefore, we conclude that the level of Gal4:VP16 protein produced by the matα driver is not limiting in the presence of two UAS-controlled transgenes and that failure of the W200A GFP-HP1a transgene to suppress the HP1a RNAi-induced PHeMAAH defects indicates that physical interaction between HP1a and Piwi is required to promote centromere proximal association of achiasmate homologs.

Discussion

HP1a and Piwi collaborate to promote the association of achiasmate homologs

In this study, we reveal a previously unknown role for heterochromatin-associated proteins in maintaining pericentric

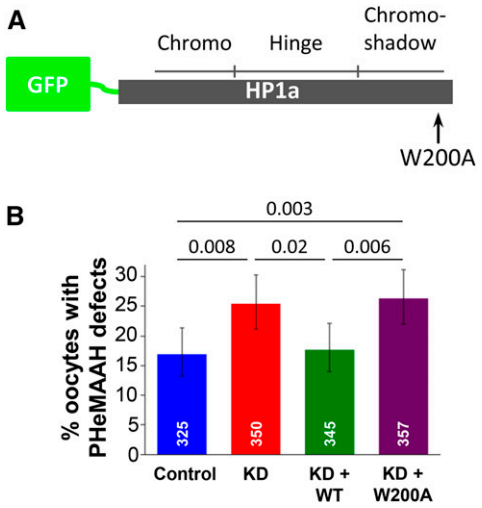

Figure 4 PHeMAAH defects induced by expression of the HP1a RNAi^{GD} hairpin can be rescued by wild-type HP1a expression but not by the W200A mutant HP1a protein. (A) UAS/Gal4-inducible transgenes were generated that encode wild-type (WT) or mutant (W200A) HP1a protein tagged with GFP at its N-terminus. The three HP1a domains are indicated, as is the site of the W200A mutation within the shadow domain. (B) "Control" oocytes carry the HP1a RNAi^{GD} transgene, but it is not expressed due to the lack of a Gal4 driver. "KD" oocytes express the hairpin under control of the matα driver. In "KD + WT" ovaries, the matα driver induces expression of the HP1a RNAi^{V20} hairpin as well as expression of GFP-tagged wild-type HP1a protein. "KD + W200A" indicates HP1a RNAi^{V20} knockdown as well as simultaneous expression of GFP-tagged HP1a protein containing the W200A mutation, which disrupts HP1a interaction with Piwi. Numbers of oocytes scored for each genotype are shown in white, and *P*-values are shown above the bars. Sixty ovarioles were scored for each genotype, and 95% confidence intervals are shown as error bars. For complete FISH data, see Table S3.

heterochromatin-mediated association of achiasmate homologs (PHeMAAH) during meiotic prophase. Reducing either HP1a or Piwi in the *Drosophila* female germline induces a significant increase in the frequency of meiotic nondisjunction of *FM7a/X* homologs, demonstrating that both proteins are required to ensure proper biorientation and segregation of achiasmate chromosomes. To test the hypothesis that increased NDJ is caused by weakening or failure of PHeMAAH, we used a FISH assay to quantitatively assess the centromere proximal association of the achiasmate *FM7a/X* homolog pair in KD and control oocytes. RNAi knockdown of either HP1a or Piwi resulted in a significant increase in the percentage of oocytes in which the pericentric region of *FM7a* was separated from the normal *X* chromosome. In *FM7a/X* flies that expressed an HP1a or Piwi RNAi hairpin in combination with an additional transgenic copy of the corresponding wild-type gene, the RNAi-induced PHeMAAH defects were reduced to levels comparable to those of controls. These data confirm that pericentric heterochromatin-mediated association of achiasmate homologs depends on a threshold level of HP1a and Piwi protein in oocytes. Because matα driver expression does not begin until mid-prophase (Weng *et al.* 2014), when homologs are already fully synapsed, our experimental strategy has allowed us to specifically monitor how reduction of HP1a or Piwi affects the maintenance of PHeMAAH. Our approach differs from that of a previous study that monitored homolog pairing at earlier stages of meiosis by examining mutant germaria (Blumenstiel *et al.* 2008). Because germarial morphology is severely disrupted in *piwi*^{1} homozygotes, analysis of pairing was not possible in this mutant background. However, mutations in other components of the piRNA pathway did not cause synapsed homologs to exhibit pairing defects during early prophase (Blumenstiel *et al.* 2008). We suspect that our knockdown strategy combined with targeted analysis of the *FM7a/X* achiasmate homolog pair during later stages of oogenesis accounts for our different findings.

Our results argue that association of achiasmate homologs also depends on H3K9 methyl marks that recruit HP1a to the pericentric heterochromatin. Previous work has demonstrated that *Su(var)3–9* mutants display defects in H3K9 methylation patterns and reduced pericentric HP1a localization in both the ovary (Schotta *et al.* 2002; Yoon *et al.* 2008) and salivary glands (Brower-Toland *et al.* 2009), and similar phenotypes have been observed in Eggless RNAi KD salivary glands (Brower-Toland *et al.* 2009). When we use the matα driver to knock down either Su(var)3–9 or Eggless protein during meiotic prophase, we observe PHeMAAH defects at levels similar to those observed in HP1a and Piwi knockdown ovaries. Therefore, our data are consistent with a model in which centromere proximal association of achiasmate homologs depends on recruitment of HP1a to the pericentric heterochromatin by H3K9 methyl marks laid down by histone methyltransferase proteins.

Because we found that both HP1a and Piwi are required for PHeMAAH, and several lines of evidence have demonstrated that Piwi binds to the HP1a dimer, we tested the hypothesis that interaction of HP1a with Piwi is required to maintain the association of achiasmate homologs. The HP1a W200A mutation prevents Piwi binding by altering the surface formed by HP1a dimerization (Brower-Toland *et al.* 2007; Mendez *et al.* 2011), while the Piwi V30A mutation is located in a pentapeptide motif (PXVXL) through which Piwi interacts with HP1a (Brower-Toland *et al.* 2007). When a transgene encoding either of these mutant proteins was expressed in conjunction with an RNAi hairpin targeting the respective wild-type endogenous protein, the mutant protein was unable to suppress the PHeMAAH defects caused by knockdown. This contrasts sharply with the rescue that we observed when a transgene encoding the corresponding wild-type protein was expressed in KD oocytes. Therefore, in two independent approaches, rescue of RNAi-induced PHeMAAH defects was eliminated by mutation of a single amino acid known to abolish the interaction of HP1a with Piwi. These data provide strong evidence that HP1a and Piwi must interact in order to keep achiasmate homologs physically together.

Weakened PHeMAAH predisposes achiasmate homologs to segregation errors

For Piwi KD oocytes, NDJ values (~16%) and PHeMAAH defects (~28%, as quantified by FISH) were reasonably well matched. However, we observed a much more pronounced

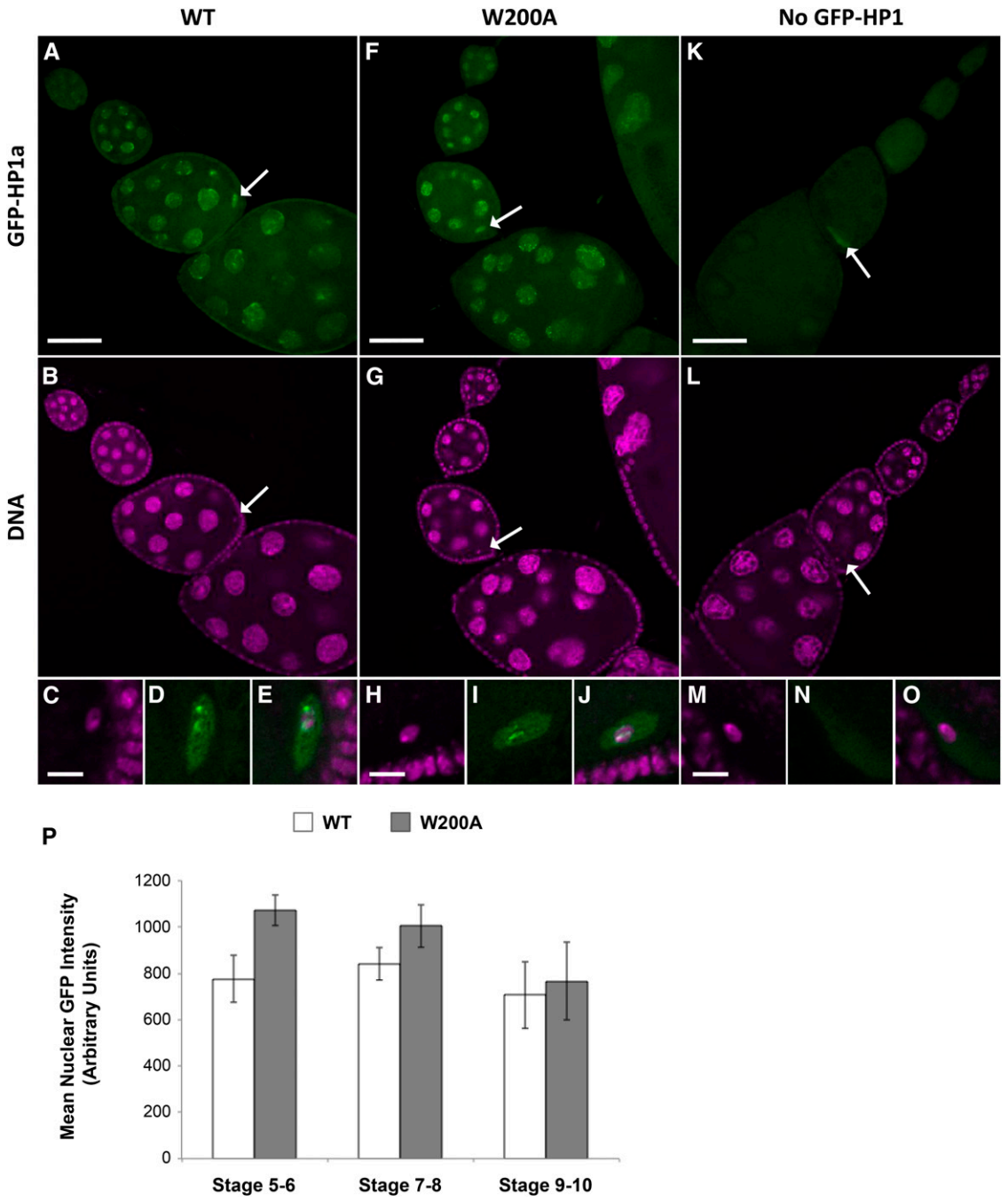

Figure 5 Wild-type and W200A GFP-HP1a protein expression levels and localization in the female germline are similar. Representative confocal images of ovarioles in which the indicated UAS-driven GFP-HP1a protein (WT or W200A) as well as the HP1a RNAi^{V20} hairpin was induced by the matα Gal4 driver. Each image represents a single confocal optical section, and image acquisition and processing were identical for all three genotypes presented. GFP fluorescence is green, and Hoechst signal (DNA) is magenta. Arrows indicate oocyte nuclei for which enlarged insets are shown in the bottom row. (A–E) Ovariole from female expressing wild-type (WT) GFP-HP1a protein. GFP signal is visible in nurse cell and oocyte nuclei. (C–E) Distinct patches of wild-type HP1a signal colocalize with the oocyte chromatin. Note that GFP signal is absent in follicle cells in which the matα driver is not expressed. (F–J) Expression of GFP-HP1a W200A mutant protein in the ovariole. GFP signal intensity in germline nuclei is comparable to that seen in wild type (compare A to F and see below). (H–J) Mutant W200A HP1a protein also localizes in distinct patches to the oocyte DNA. (K–O) Ovariole from control female lacking GFP-HP1a expression because the matα driver is absent. In this genotype, weak signal is often visible in the oocyte cytosol, most likely due to autofluorescence. However, note the absence of GFP signal associated with nurse cell or oocyte chromatin. Scale bars correspond to 50 μm in A, F, and K and 5 μm in C, H, and M. (P) Quantification of nuclear GFP signal demonstrates that the lack of rescue observed in W200A GFP-HP1a-expressing flies is not due to insufficient transgene expression. Each bar represents the average GFP intensity for nurse cell nuclei within three representative egg chambers for each genotype at the specified stage of oogenesis (see *Materials and Methods*). Error bars represent SD. *P*-values comparing wild type and W200A were calculated using an unpaired *t*-test ($P = 0.01$ for stage 5–6, $P = 0.15$ for stage 7–8, and $P = 0.62$ for stage 9–10).

difference between the severity of NDJ and FISH phenotypes in HP1a KD oocytes, with approximately 1.7% chromosome missegregation in NDJ tests compared to roughly 23% separated FISH signals in oocytes. In addition, the baseline value for separated *FM7a/X* pericentric heterochromatin in both HP1a and Piwi control oocytes hovered between 10 and 15% in most of our FISH experiments, but NDJ was considerably lower (0.33% for the HP1a control and 1.44% for the Piwi control). This means that weakened PHeMAAH between a pair of homologs during prophase I does not always result in missegregation during anaphase I. Our previous work has shown that a reduction of pericentric heterochromatin on one of the chromosomes of an achiasmate *X* chromosome pair sensitizes it to missegregation under conditions that perturb PHeMAAH (Subramanian and Bickel 2009). This is the case for the *FM7a/X* achiasmate chromosome pair that we have used in our analyses. However, we cannot rule out the possibility that the large distal block of heterochromatin on *FM7a*, even when removed from a centromere proximal location, still may contribute to accurate segregation of the achiasmate *FM7a/X* pair. Another possibility is that the physical separation of pericentric regions that we observe when HP1a levels are reduced does not reflect complete disengagement of the achiasmate homologs. This idea is reinforced by the observation that during prometaphase, achiasmate chromosomes move toward the poles but rejoin the chiasmate bivalents at the spindle equator by metaphase (Gilliland *et al.* 2009). Hawley and colleagues have observed heterochromatin threads that stretch between separated achiasmate homologs during prometaphase and have proposed that congression back to the metaphase plate is mediated by contraction of these threads (Hughes *et al.* 2009). Reducing topoisomerase II activity in mature oocytes disrupts the normal morphology of heterochromatin threads and separation of achiasmate homologs during prometaphase, suggesting that DNA entanglements also play a role in heterochromatin-mediated association (Hughes and Hawley 2014).

We suggest that the "two-spot" FISH phenotype that we observe in control oocytes represents an elastic state in which the bulk of pericentric heterochromatin for the two homologs has separated but that homologs remain physically connected by stretched heterochromatin threads that are not readily apparent in our FISH assay. The increased frequency of the "two-spot" phenotype observed in KD oocytes reflects weakened PHeMAAH and looser association between homologs. Indeed, HP1a knockdown most likely reduces the compaction of heterochromatin resulting in a less rigid state. However, even when levels of HP1a are reduced, most homologs remain connected by heterochromatin threads and are able to segregate correctly. Our finding that reduction of HP1a induces a significant elevation in chromosome segregation errors argues that increased stretching of pericentric heterochromatin can cause missegregation for a subset of chromosome pairs. Therefore, we conclude that weakened centromere proximal association predisposes the *FM7a/X* homolog pair to missegregation but does not guarantee it.

Interestingly, HP1a and Piwi KD oocytes that have disassembled their synaptonemal complex exhibit the most dramatic increase in PHeMAAH defects, but we do observe separation of *FM7a/X* pericentric heterochromatin at stages where the synaptonemal complex is still intact. Moreover, clustering of oocyte centromeres persists even after synaptonemal complex disassembly in wild-type oocytes (Takeo *et al.* 2011). These results suggest that even within the context of the synaptonemal complex or centromeric clustering, the elasticity of pericentric heterochromatin can allow this region of the *FM7a* homolog to stretch away from its partner. This most likely occurs because the *FM7a/X* homolog pair provides a sensitized system to detect PHeMAAH defects given that pericentric heterochromatin is substantially reduced on the *FM7a* chromosome. Supporting this idea, HP1a KD did not cause detectable PHeMAAH defects between a normal *X* chromosome and *In(1)dl-49*, an *X* chromosome derivative that carries euchromatic inversions that suppress recombination but contains un-rearranged full-length pericentric heterochromatin (data not shown).

A model for HP1a-Piwi interaction in PHeMAAH

Previously published work has demonstrated that the yeast HP1a ortholog Swi6 forms dimers that can bridge two nucleosomes, with each chromodomain binding to a different histone H3 tail (Canzio *et al.* 2011). Interaction of human HP1α dimers with a single molecule of nucleosome-associated DNA can cause its compaction *in vitro*, and dimerization of *Drosophila* HP1a can facilitate looping within chromosomes *in vivo*, bringing distantly spaced regions of the chromosome into close proximity (Azzaz *et al.* 2014). Moreover, *in vitro* experiments have demonstrated that two separate nucleosomal DNA arrays are held together when HP1α dimers are present but remain separate when incubated with mutant HP1α proteins that cannot dimerize (Azzaz *et al.* 2014). With these observations in mind, we propose a speculative model suggesting how HP1a, H3K9 methylation, and Piwi may be working together to bring about the stable association of achiasmate homologous chromosomes during meiotic prophase (Figure 6). In this model, the chromodomains of an HP1a dimer bind to nucleosomes at the H3K9 methyl mark, with dimers physically tethering homologous chromosomes as they do with *in vitro* nucleosome arrays. HP1a bridging of homologs must be restricted to regions of homologous heterochromatin, and we suggest that Piwi provides this function, with Piwi-associated RNA molecules interacting with DNA and thereby providing sequence recognition. In addition, the inability of W200A HP1a dimers to mediate PHeMAAH independently of Piwi interaction suggests that Piwi also may be required to initiate or stabilize HP1a bridging.

Figure 6 illustrates two different scenarios that rely on recruitment of HP1a to H3K9 methyl marks, HP1a dimerization and interaction with Piwi, as well as interaction of Piwi-bound RNA with the pericentric heterochromatin of homologous chromosomes. One possibility (Figure 6A) is that Piwi binds an RNA that directly hybridizes with the DNA,

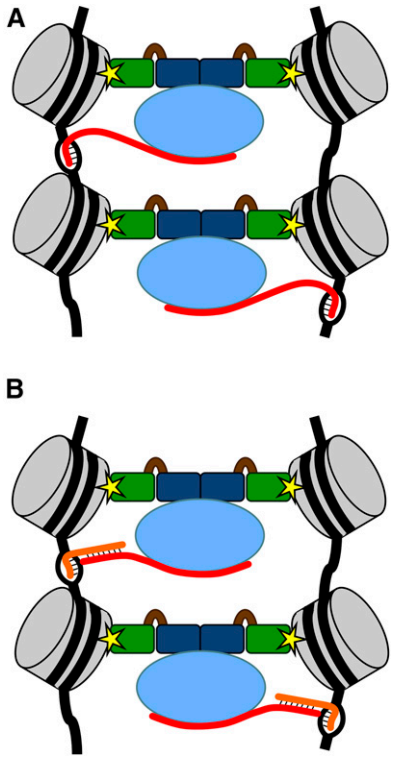

Figure 6 A model illustrating possible roles for HP1a and Piwi in PHeMAAH. In this model, nucleosomes (gray) from two homologs are physically connected by dimers of HP1a. HP1a chromodomains (green) bind to the chromatin at the H3K9 methyl mark (yellow star) and dimerize via interactions at their CSDs (dark blue). Piwi (light blue), along with an associated RNA (red), binds to the HP1a dimer at the CSD-CSD surface. The Piwi-associated RNA provides sequence specificity by interacting with the DNA sequence via (A) RNA-DNA hybridzation or (B) hybridization to a second RNA (orange), such as a nascent transcript, emerging from the DNA (black).

with RNA-DNA interactions occurring on both homologs such that stable HP1a bridging occurs only if both chromosomes are able to hybridize with the Piwi-associated RNA. Because pericentric satellite sequences are highly repetitive, a small number of RNA sequences may be sufficient to direct the HP1a-Piwi complex to a relatively large region of heterochromatin. Alternatively (Figure 6B), the Piwi-associated RNA could be interacting with DNA sequences via another RNA intermediate, such as a nascent satellite sequence transcript. Though not included in this model, it is interesting to note that like *Drosophila* HP1a, mammalian HP1α and *Schizosaccharomyces pombe* Swi6 also bind RNA (Muchardt *et al.* 2002; Keller *et al.* 2012). This activity is required in mammals for the targeting of HP1α to the pericentric heterochromatin, raising the possibility that in the context of PHeMAAH, HP1a-RNA interactions also could contribute to targeting or stabilizing the HP1a-Piwi complex.

Both versions of the model presented in Figure 6 rely on interaction between Piwi and RNA to provide the homology recognition that is essential for PHeMAAH. At this time, our suggestion that Piwi-bound RNA is required for PHeMAAH is based solely on extrapolation of published evidence detailing Piwi-piRNA interactions (Le Thomas *et al.* 2013; Mani and Juliano 2013; Ku and Lin 2014). We can only speculate on the identity of Piwi-associated RNAs that might be involved in PHeMAAH and whether these might be mature piRNAs or unprocessed nuclear transcripts. piRNAs largely originate from transcription of piRNA clusters enriched in heterochromatic regions, and long piRNA precursor molecules in excess of 200 nucleotides have been detected by RT-PCR (Pal-Bhadra *et al.* 2004; Saito *et al.* 2006; Brennecke *et al.* 2007; Usakin *et al.* 2007). After processing in the cytosol, mature piRNAs are loaded onto Piwi and transported back into the nucleus, where they are thought to guide Piwi to retrotransposon sequences throughout the genome (Brennecke *et al.* 2007; Huang *et al.* 2013; Weick and Miska 2014). In addition, RNA transcripts from both strands of the pericentric satellite DNA of all *Drosophila* chromosomes have been detected, including the 359-bp satellite sequence on the *X* chromosome (Usakin *et al.* 2007). Furthermore, pericentric repeat sequences have been detected among small RNAs bound to Piwi (Brennecke *et al.* 2007), raising the possibility that RNA molecules from these regions may contribute to homology recognition by the HP1a-Piwi complex. Further work will be required to establish whether RNA binding is required for Piwi to promote PHeMAAH and, if so, how those RNAs are generated and processed.

The proposal that Piwi facilitates the association of homologous sequences on different chromosomes is not without precedent. Piwi has been implicated previously in a phenomenon known as *pairing-sensitive silencing* in which transcriptional repression of transgenes on homologous chromosomes occurs only when they are able to pair (Kassis *et al.* 1991). In their analysis of transgenes carrying the *Fab-7* silencing element upstream of a miniwhite reporter, Grimaud *et al.* (2006) found that pairing-sensitive silencing was disrupted in *piwi*^{1} and *piwi*^{2} mutant adults, resulting in an increase in eye pigmentation. In addition, production of short RNAs from the *Fab-7* region of the paired transgenes was strongly reduced by *piwi* mutations. Although the mechanism of pairing-sensitive silencing is not completely understood, these results suggest that Piwi, with the guidance of small RNAs, can promote pairing between homologous regions of different chromosomes in a way that is similar to the mechanism that we envision for Piwi in our model of PHeMAAH (Figure 6). Our chromosome spread analysis indicates that Piwi stably localizes at many locations along the meiotic chromosomes, including the centromere proximal regions. Therefore, Piwi protein is in the right place at the right time to collaborate with HP1a and promote the sustained association of pericentric regions of achiasmate homologs during meiotic prophase.

Possible relevance to human biology

In humans, chromosome segregation errors lead to trisomy disorders, including Down syndrome, and are the leading cause of miscarriages (Nagaoka *et al.* 2012). Although direct evidence for the existence of an achiasmate chromosome association system in humans is lacking, multiple lines of inquiry indicate that human chromosomes frequently fail to recombine

but are still able to segregate correctly (Oliver *et al.* 2008; Cheng *et al.* 2009; Fledel-Alon *et al.* 2009; Nagaoka *et al.* 2012). HP1a, Su(var)3–9, and Piwi are highly conserved (Saunders *et al.* 1993; Cox *et al.* 1998; Aagaard *et al.* 1999), and human Su(var)3–9 and HP1 proteins are able to functionally replace their *Drosophila* counterparts (Ma *et al.* 2001; Schotta *et al.* 2002). Therefore, if a human achiasmate segregation system does indeed exist and it relies on pericentric heterochromatin-mediated association of homologs, these three proteins may function as conserved components of this pathway. Our findings that HP1a and Piwi must collaborate to promote PHeMAAH in *Drosophila* oocytes opens the door to further investigation of the mechanisms that govern achiasmate chromosome segregation in flies and possibly even in humans.

Acknowlegments

We thank S. Elgin for providing the wild-type and mutant Piwi transgene stocks and W. Theurkauf for providing anti-Piwi antibodies. We are grateful to the Bloomington *Drosophila* Stock Center (NIH P40-OD018537), the Vienna *Drosophila* RNAi Center, and the Harvard Transgenic RNAi Project (NIH/NIGMS R01-GM084947) for providing the stocks necessary for this study and the *Drosophila* Genome Resource Center (supported by NIH grant 2P40OD010949-10A1) for supplying the HP1a cDNA. We acknowledge Brian Seitz for generating the w^{1118} B^{1} chromosome used for the Piwi NDJ tests and Charlotte Jeffreys for help with the Piwi NDJ tests. We thank Viji Subramanian and members of the Bickel laboratory for helpful discussions and critical reading of the manuscript. The confocal microscope used in this study was purchased with an MRI award from the National Science Foundation (DBI-1039423). This work was funded by the National Science Foundation (grant MCB-0919893) and the National Institutes of Health (grant R01-GM59354 awarded to S.E.B.).

Literature Cited

Aagaard, L., G. Laible, P. Selenko, M. Schmid, R. Dorn *et al.*, 1999 Functional mammalian homologues of the *Drosophila* PEV-modifier *Su(var)3–9* encode centromere-associated proteins which complex with the heterochromatin component M31. EMBO J. 18: 1923–1938.

Agresti, A., and B. A. Coull, 1998 Approximate is better than "exact" for interval estimation of binomial proportions. Am. Stat. 52: 119–126.

Americo, J., M. Whiteley, J. L. Brown, M. Fujioka, J. B. Jaynes *et al.*, 2002 A complex array of DNA-binding proteins required for pairing-sensitive silencing by a polycomb group response element from the Drosophila *engrailed* gene. Genetics 160: 1561–1571.

Ashburner, M., K. Golic, and R. Hawley, 2005 *Drosophila: A Laboratory Handbook*. Cold Spring Harbor Laboratory Press, Cold Spring Harbor, New York.

Azzaz, A. M., M. W. Vitalini, A. S. Thomas, J. P. Price, M. J. Blacketer *et al.*, 2014 Human heterochromatin protein 1α promotes nucleosome associations that drive chromatin condensation. J. Biol. Chem. 289: 6850–6861.

Bickel, S. E., T. Orr-Weaver, and E. M. Balicky, 2002 The sister-chromatid cohesion protein ORD is required for chiasma maintenance in *Drosophila* oocytes. Curr. Biol. 12: 925–929.

Bischof, J., R. K. Maeda, M. Hediger, F. Karch, and K. Basler, 2007 An optimized transgenesis system for *Drosophila* using germ-line-specific phiC31 integrases. Proc. Natl. Acad. Sci. USA 104: 3312–3317.

Blower, M. D., and G. H. Karpen, 2001 The role of *Drosophila* CID in kinetochore formation, cell-cycle progression and heterochromatin interactions. Nat. Cell Biol. 3: 730–739.

Blumenstiel, J. P., R. Fu, W. E. Theurkauf, and R. S. Hawley, 2008 Components of the RNAi machinery that mediate long-distance chromosomal associations are dispensable for meiotic and early somatic homolog pairing in *Drosophila melanogaster*. Genetics 180: 1355–1365.

Brennecke, J., A. A. Aravin, A. Stark, M. Dus, M. Kellis *et al.*, 2007 Discrete small RNA-generating loci as master regulators of transposon activity in *Drosophila*. Cell 128: 1089–1103.

Brower-Toland, B., S. D. Findley, L. Jiang, L. Liu, H. Yin *et al.*, 2007 *Drosophila* PIWI associates with chromatin and interacts directly with HP1a. Genes Dev. 21: 2300–2311.

Brower-Toland, B., N. C. Riddle, H. Jiang, K. L. Huisinga, and S. C. Elgin, 2009 Multiple SET methyltransferases are required to maintain normal heterochromatin domains in the genome of *Drosophila melanogaster*. Genetics 181: 1303–1319.

Buonomo, S. B., R. K. Clyne, J. Fuchs, J. Loidl, F. Uhlmann *et al.*, 2000 Disjunction of homologous chromosomes in meiosis I depends on proteolytic cleavage of the meiotic cohesin Rec8 by separin. Cell 103: 387–398.

Canzio, D., E. Y. Chang, S. Shankar, K. M. Kuchenbecker, M. D. Simon *et al.*, 2011 Chromodomain-mediated oligomerization of HP1 suggests a nucleosome-bridging mechanism for heterochromatin assembly. Mol. Cell 41: 67–81.

Canzio, D., A. Larson, and G. J. Narlikar, 2014 Mechanisms of functional promiscuity by HP1 proteins. Trends Cell Biol. 24: 377–386.

Cheng, E. Y., P. A. Hunt, T. A. Naluai-Cecchini, C. L. Fligner, V. Y. Fujimoto *et al.*, 2009 Meiotic recombination in human oocytes. PLoS Genet. 5: e1000661.

Cox, D. N., A. Chao, J. Baker, L. Chang, D. Qiao *et al.*, 1998 A novel class of evolutionarily conserved genes defined by piwi are essential for stem cell self-renewal. Genes Dev. 12: 3715–3727.

Darricarrère, N., N. Liu, T. Watanabe, and H. Lin, 2013 Function of Piwi, a nuclear Piwi/Argonaute protein, is independent of its slicer activity. Proc. Natl. Acad. Sci. USA 110: 1297–1302.

Dernburg, A. F., J. W. Sedat, and R. S. Hawley, 1996 Direct evidence of a role for heterochromatin in meiotic chromosome segregation. Cell 86: 135–146.

Dufourt, J., C. Dennis, A. Boivin, N. Gueguen, E. Théron *et al.*, 2014 Spatio-temporal requirements for transposable element piRNA-mediated silencing during *Drosophila* oogenesis. Nucleic Acids Res. 42: 2512–2524.

Eissenberg, J. C., G. D. Morris, G. Reuter, and T. Hartnett, 1992 The heterochromatin-associated protein HP-1 is an essential protein in Drosophila with dosage-dependent effects on position-effect variegation. Genetics 131: 345–352.

Fledel-Alon, A., D. J. Wilson, K. Broman, X. Wen, C. Ober *et al.*, 2009 Broad-scale recombination patterns underlying proper disjunction in humans. PLoS Genet. 5: e1000658.

Gilliland, W. D., S. F. Hughes, D. R. Vietti, and R. S. Hawley, 2009 Congression of achiasmate chromosomes to the metaphase plate in *Drosophila melanogaster* oocytes. Dev. Biol. 325: 122–128.

Gong, W. J., K. S. McKim, and R. S. Hawley, 2005 All paired up with no place to go: pairing, synapsis, and DSB formation in a balancer heterozygote. PLoS Genet. 1: e67.

Grell, R., 1976 Distributive pairing, pp. 436–486 in *The Genetics and Biology of Drosophila*, edited by M. Ashburner, and E. Novitski. Academic Press, New York.

Grimaud, C., F. Bantignies, M. Pal-Bhadra, P. Ghana, U. Bhadra *et al.*, 2006 RNAi components are required for nuclear clustering of Polycomb group response elements. Cell 124: 957–971.

Gu, T., and S. C. Elgin, 2013 Maternal depletion of Piwi, a component of the RNAi system, impacts heterochromatin formation in *Drosophila*. PLoS Genet. 9: e1003780.

Hawley, R. S., H. Irick, D. A. Haddox, M. D. Whiteley, T. Arbel *et al.*, 1992 There are two mechanisms of achiasmate segregation in *Drosophila* females, one of which requires heterochromatic homology. Dev. Genet. 13: 440–467.

Hodges, C. A., E. Revenkova, R. Jessberger, T. J. Hassold, and P. A. Hunt, 2005 SMC1beta-deficient female mice provide evidence that cohesins are a missing link in age-related nondisjunction. Nat. Genet. 37: 1351–1355.

Hsieh, T., and D. Brutlag, 1979 Sequence and sequence variation within the 1.688 g/cm^3 satellite DNA of *Drosophila melanogaster*. J. Mol. Biol. 135: 465–481.

Huang, X. A., H. Yin, S. Sweeney, D. Raha, M. Snyder *et al.*, 2013 A major epigenetic programming mechanism guided by piRNAs. Dev. Cell 24: 502–516.

Hughes, S. E., and R. S. Hawley, 2014 Topoisomerase II is required for the proper separation of heterochromatic regions during *Drosophila melanogaster* female meiosis. PLoS Genet. 10: e1004650.

Hughes, S. E., W. D. Gilliland, J. L. Cotitta, S. Takeo, K. A. Collins *et al.*, 2009 Heterochromatic threads connect oscillating chromosomes during prometaphase I in *Drosophila* oocytes. PLoS Genet. 5: e1000348.

James, T. C., J. C. Eissenberg, C. Craig, V. Dietrich, A. Hobson *et al.*, 1989 Distribution patterns of HP1, a heterochromatin-associated nonhistone chromosomal protein of Drosophila. Eur. J. Cell Biol. 50: 170–180.

Januschke, J., L. Gervais, S. Dass, J. A. Kaltschmidt, H. Lopez-Schier *et al.*, 2002 Polar transport in the *Drosophila* oocyte requires Dynein and Kinesin I cooperation. Curr. Biol. 12: 1971–1981.

Karpen, G. H., M. H. Le, and H. Le, 1996 Centric heterochromatin and the efficiency of achiasmate disjunction in *Drosophila* female meiosis. Science 273: 118–122.

Kassis, J. A., 1994 Unusual properties of regulatory DNA from the Drosophila engrailed gene: three "pairing-sensitive" sites within a 1.6-kb region. Genetics 136: 1025–1038.

Kassis, J. A., E. P. VanSickle, and S. M. Sensabaugh, 1991 A fragment of *engrailed* regulatory DNA can mediate transvection of the *white* gene in Drosophila. Genetics 128: 751–761.

Keller, C., R. Adaixo, R. Stunnenberg, K. J. Woolcock, S. Hiller *et al.*, 2012 HP1(Swi6) mediates the recognition and destruction of heterochromatic RNA transcripts. Mol. Cell 47: 215–227.

Khetani, R. S., and S. E. Bickel, 2007 Regulation of meiotic cohesion and chromosome core morphogenesis during pachytene in *Drosophila* oocytes. J. Cell Sci. 120: 3123–3137.

Klattenhoff, C., H. Xi, C. Li, S. Lee, J. Xu *et al.*, 2009 The *Drosophila* HP1 homolog Rhino is required for transposon silencing and piRNA production by dual-strand clusters. Cell 138: 1137–1149.

Krauss, V., and G. Reuter, 2000 Two genes become one: the genes encoding heterochromatin protein Su(var)3–9 and translation initiation factor subunit eIF-2γ are joined to a dicistronic unit in holometabolic insects. Genetics 156: 1157–1167.

Ku, H. Y., and H. Lin, 2014 PIWI proteins and their interactors in piRNA biogenesis, germline development and gene expression. Natl. Sci. Rev. 1: 205–218.

Le Thomas, A., A. K. Rogers, A. Webster, G. K. Marinov, S. E. Liao *et al.*, 2013 Piwi induces piRNA-guided transcriptional silencing and establishment of a repressive chromatin state. Genes Dev. 27: 390–399.

Lipsick, J., 2010 P{GFP-HP1} construct and insertion. Available at: http://flybase.org/reports/FBrf0210709.html.

Ma, J., K. K. Hwang, H. J. Worman, J. C. Courvalin, and J. C. Eissenberg, 2001 Expression and functional analysis of three isoforms of human heterochromatin-associated protein HP1 in *Drosophila*. Chromosoma 109: 536–544.

Mani, S. R., and C. E. Juliano, 2013 Untangling the web: the diverse functions of the PIWI/piRNA pathway. Mol. Reprod. Dev. 80: 632–664.

Mendez, D. L., D. Kim, M. Chruszcz, G. E. Stephens, W. Minor *et al.*, 2011 The HP1a disordered C terminus and chromo shadow domain cooperate to select target peptide partners. Chembiochem 12: 1084–1096.

Mendez, D. L., R. E. Mandt, and S. C. Elgin, 2013 Heterochromatin protein 1a (HP1a) partner specificity is determined by critical amino acids in the chromo shadow domain and C-terminal extension. J. Biol. Chem. 288: 22315–22323.

Moore, D. P., W. Y. Miyazaki, J. E. Tomkiel, and T. L. Orr-Weaver, 1994 Double or nothing: a Drosophila mutation affecting meiotic chromosome segregation in both females and males. Genetics 136: 953–964.

Muchardt, C., M. Guilleme, J. S. Seeler, D. Trouche, A. Dejean *et al.*, 2002 Coordinated methyl and RNA binding is required for heterochromatin localization of mammalian HP1α. EMBO Rep. 3: 975–981.

Nagaoka, S. I., T. J. Hassold, and P. A. Hunt, 2012 Human aneuploidy: mechanisms and new insights into an age-old problem. Nat. Rev. Genet. 13: 493–504.

Oliver, T. R., E. Feingold, K. Yu, V. Cheung, S. Tinker *et al.*, 2008 New insights into human nondisjunction of chromosome 21 in oocytes. PLoS Genet. 4: e1000033.

Page, S. L., and R. S. Hawley, 2001 *c(3)G* encodes a *Drosophila* synaptonemal complex protein. Genes Dev. 15: 3130–3143.

Page, S. L., R. S. Khetani, C. M. Lake, R. J. Nielsen, J. K. Jeffress *et al.*, 2008 *corona* is required for higher-order assembly of transverse filaments into full-length synaptonemal complex in Drosophila oocytes. PLoS Genet. 4: e1000194.

Pal-Bhadra, M., B. A. Leibovitch, S. G. Gandhi, M. R. Chikka, M. Rao *et al.*, 2004 Heterochromatic silencing and HP1 localization in *Drosophila* are dependent on the RNAi machinery. Science 303: 669–672.

Peters, A. H., A. W. Plug, M. J. van Vugt, and P. de Boer, 1997 A drying-down technique for the spreading of mammalian meiocytes from the male and female germline. Chromosome Res. 5: 66–68.

Saito, K., K. M. Nishida, T. Mori, Y. Kawamura, K. Miyoshi *et al.*, 2006 Specific association of Piwi with rasiRNAs derived from retrotransposon and heterochromatic regions in the *Drosophila* genome. Genes Dev. 20: 2214–2222.

Saunders, W. S., C. Chue, M. Goebl, C. Craig, R. F. Clark *et al.*, 1993 Molecular cloning of a human homologue of Drosophila heterochromatin protein HP1 using anti-centromere autoantibodies with anti-chromo specificity. J. Cell Sci. 104: 573–582.

Schotta, G., A. Ebert, V. Krauss, A. Fischer, J. Hoffmann *et al.*, 2002 Central role of *Drosophila* SU(VAR)3–9 in histone H3–K9 methylation and heterochromatic gene silencing. EMBO J. 21: 1121–1131.

Sentmanat, M. F., and S. C. Elgin, 2012 Ectopic assembly of heterochromatin in *Drosophila melanogaster* triggered by transposable elements. Proc. Natl. Acad. Sci. USA 109: 14104–14109.

Subramanian, V. V., and S. E. Bickel, 2009 Heterochromatin-mediated association of achiasmate homologues declines with age when cohesion is compromised. Genetics 181: 1207–1218.

Takeo, S., C. M. Lake, E. Morais-de-Sá, C. E. Sunkel, and R. S. Hawley, 2011 Synaptonemal complex-dependent centromeric clustering and the initiation of synapsis in *Drosophila* oocytes. Curr. Biol. 21: 1845–1851.

Takeo, S., S. K. Swanson, K. Nandanan, Y. Nakai, T. Aigaki *et al.*, 2012 Shaggy/glycogen synthase kinase 3β and phosphorylation of Sarah/regulator of calcineurin are essential for completion of *Drosophila* female meiosis. Proc. Natl. Acad. Sci. USA 109: 6382–6389.

Theurkauf, W. E., and R. S. Hawley, 1992 Meiotic spindle assembly in Drosophila females: behavior of nonexchange chromosomes and the effects of mutations in the *nod* kinesin-like protein. J. Cell Biol. 116: 1167–1180.

Usakin, L., J. Abad, V. V. Vagin, B. de Pablos, A. Villasante *et al.*, 2007 Transcription of the 1.688 satellite DNA family is under the control of RNA interference machinery in *Drosophila melanogaster* ovaries. Genetics 176: 1343–1349.

Vermaak, D., and H. S. Malik, 2009 Multiple roles for heterochromatin protein 1 genes in *Drosophila*. Annu. Rev. Genet. 43: 467–492.

Wang, S. H., and S. C. Elgin, 2011 *Drosophila* Piwi functions downstream of piRNA production mediating a chromatin-based transposon silencing mechanism in female germ line. Proc. Natl. Acad. Sci. USA 108: 21164–21169.

Webber, H. A., L. Howard, and S. E. Bickel, 2004 The cohesion protein ORD is required for homologue bias during meiotic recombination. J. Cell Biol. 164: 819–829.

Weick, E. M., and E. A. Miska, 2014 piRNAs: from biogenesis to function. Development 141: 3458–3471.

Wen, H., L. Andrejka, J. Ashton, R. Karess, and J. S. Lipsick, 2008 Epigenetic regulation of gene expression by *Drosophila* Myb and E2F2-RBF via the Myb-MuvB/dREAM complex. Genes Dev. 22: 601–614.

Weng, K. A., C. A. Jeffreys, and S. E. Bickel, 2014 Rejuvenation of meiotic cohesion in oocytes during prophase I is required for chiasma maintenance and accurate chromosome segregation. PLoS Genet. 10: e1004607.

Whyte, W. L., H. Irick, T. Abel, G. Yasuda, R. L. French *et al.*, 1993 The genetic analysis of achiasmate segregation in Drosophila melanogaster. III. The wild-type product of the *Axs* gene is required for the meiotic segregation of achiasmate homologs. Genetics 134: 825–835.

Yoon, J., K. S. Lee, J. S. Park, K. Yu, S. G. Paik *et al.*, 2008 dSETDB1 and SU(VAR)3–9 sequentially function during germline-stem cell differentiation in *Drosophila melanogaster*. PLoS One 3: e2234.

Zeng, W., A. R. Ball, Jr., and K. Yokomori, 2010a HP1: heterochromatin binding proteins working the genome. Epigenetics 5: 287–292.

Zeng, Y., H. Li, N. M. Schweppe, R. S. Hawley, and W. D. Gilliland, 2010b Statistical analysis of nondisjunction assays in Drosophila. Genetics 186: 505–513.

Communicating editor: J. Sekelsky

GENETICS

Supporting Information
www.genetics.org/cgi/data/genetics.115.186460/DC1/

Heterochromatin-Associated Proteins HP1a and Piwi Collaborate to Maintain the Association of Achiasmate Homologs in *Drosophila* Oocytes

Christopher C. Giauque and Sharon E. Bickel

DOI: 10.1534/genetics.115.186460

A

Maternal Chromosome(s)	Paternal Chromosomes: X^Y (y^+)	Paternal Chromosomes: 0
Normal: y w	y^+ female	y male
Normal: FM7a (y)	y^+ female	y male
Diplo: FM7a/FM7a	Dead	y female
Diplo: FM7a/y w	Dead	y female
Diplo: y w/y w	Dead	y female
Nullo: 0	y^+ male	Dead

B

Maternal Chromosome(s)	Paternal Chromosomes: X^Y (B^+)	Paternal Chromosomes: 0
Normal: w B	$B^{+/-}$ female	B male
Normal: FM7a (B)	$B^{+/-}$ female	B male
Diplo: FM7a/FM7a	Dead	B female
Diplo: FM7a/w B	Dead	B female
Diplo: w B/w B	Dead	B female
Nullo: 0	B^+ male	Dead

Figure S1. Scoring methods used for nondisjunction assays. (A) For *Su(var)205^5/+* and HP1a RNAi^{GD} NDJ tests, *FM7a/y w* females were crossed to males carrying an attached *X^Y* chromosome marked with a wild-type copy of the *yellow* gene. Body color and sex were used to distinguish progeny arising from normal, Diplo-*X* or Nullo-*X* female gametes. (B) The Piwi RNAi^{V20} NDJ tests utilized *FM7a/w B* females crossed to males that harbored an attached *X^Y* chromosome carrying a wild-type allele of the *Bar* gene. This scheme allowed us to distinguish progeny arising from normal, Diplo-*X* or Nullo-*X* eggs based on eye shape and sex.

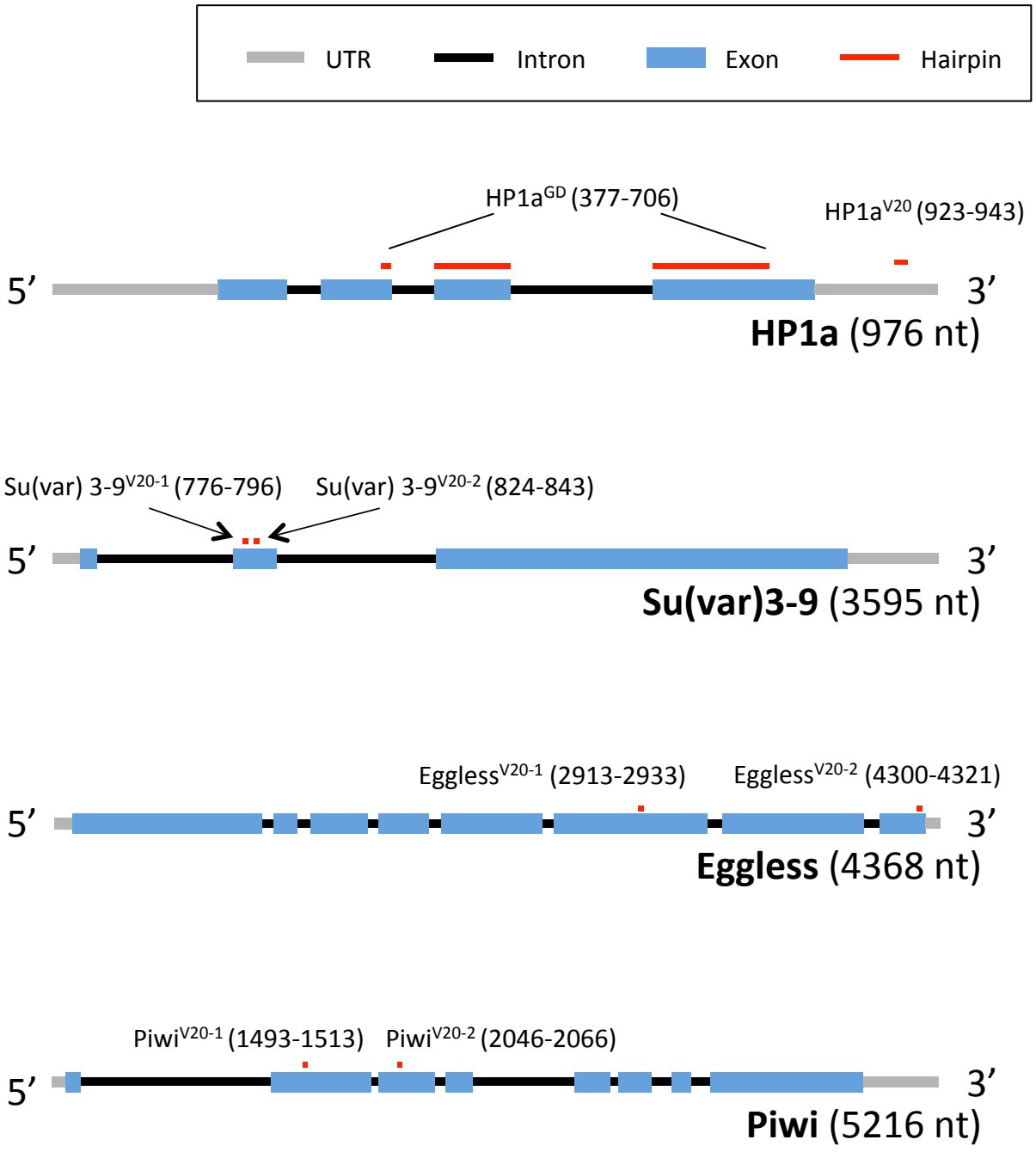

Figure S2. RNAi hairpins used in this study. A schematic is shown for each mRNA targeted for knockdown. The nucleotide length of each transcription unit is listed in parentheses after its name. Two hairpins were utilized to target each mRNA. The region targeted by each hairpin is shown in red, and the hairpin name and the specific bases targeted by the hairpin are shown directly above each mRNA. For HP1a RNAi^{GD}, the hairpin sequence spans three exons.

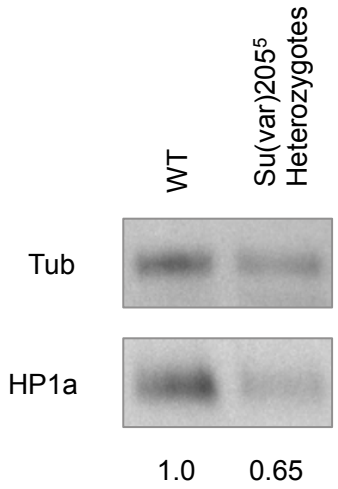

Figure S3. Heterozygotes carrying a null mutation in Su(var)205 express less HP1a in the ovary than siblings lacking the mutation. An immunoblot comparing ovary extracts from *Su(var)205*^{5} heterozygotes and from wild-type siblings from the same cross demonstrates reduced HP1a protein levels in the mutants. For each genotype, the intensity of the HP1a signal was normalized to the tubulin signal. Numbers below each lane represent the mean intensity of the signals, relative to WT, from multiple experiments (n=4).

A

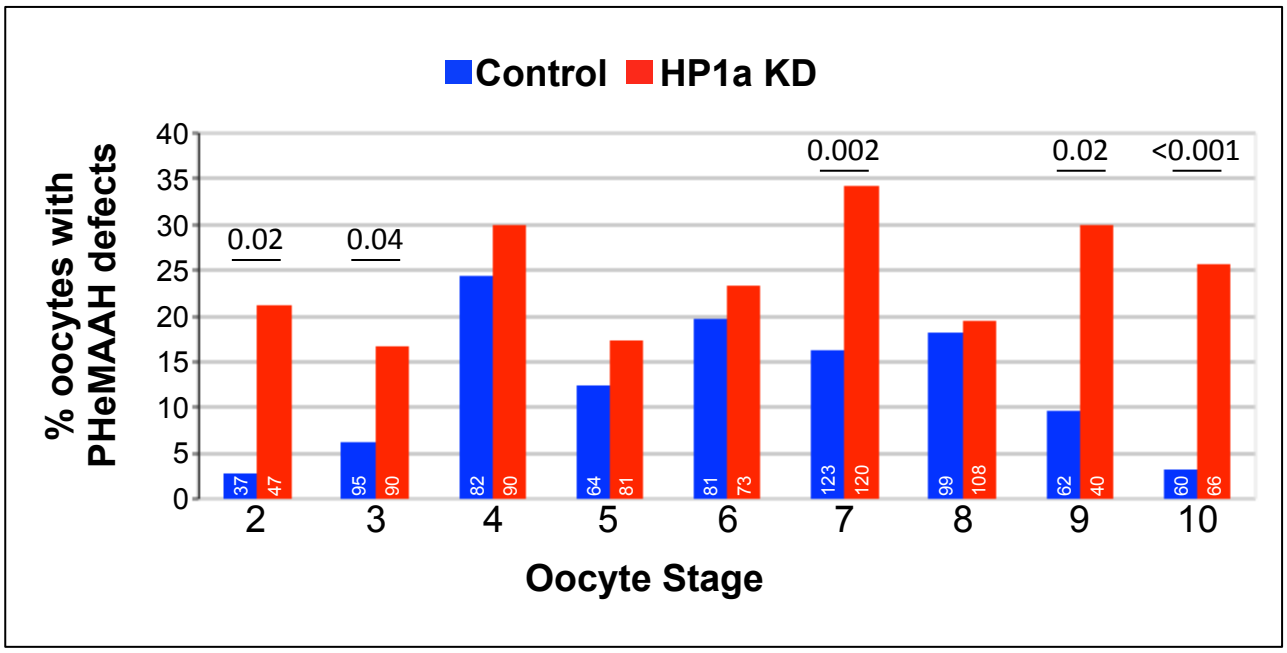

B

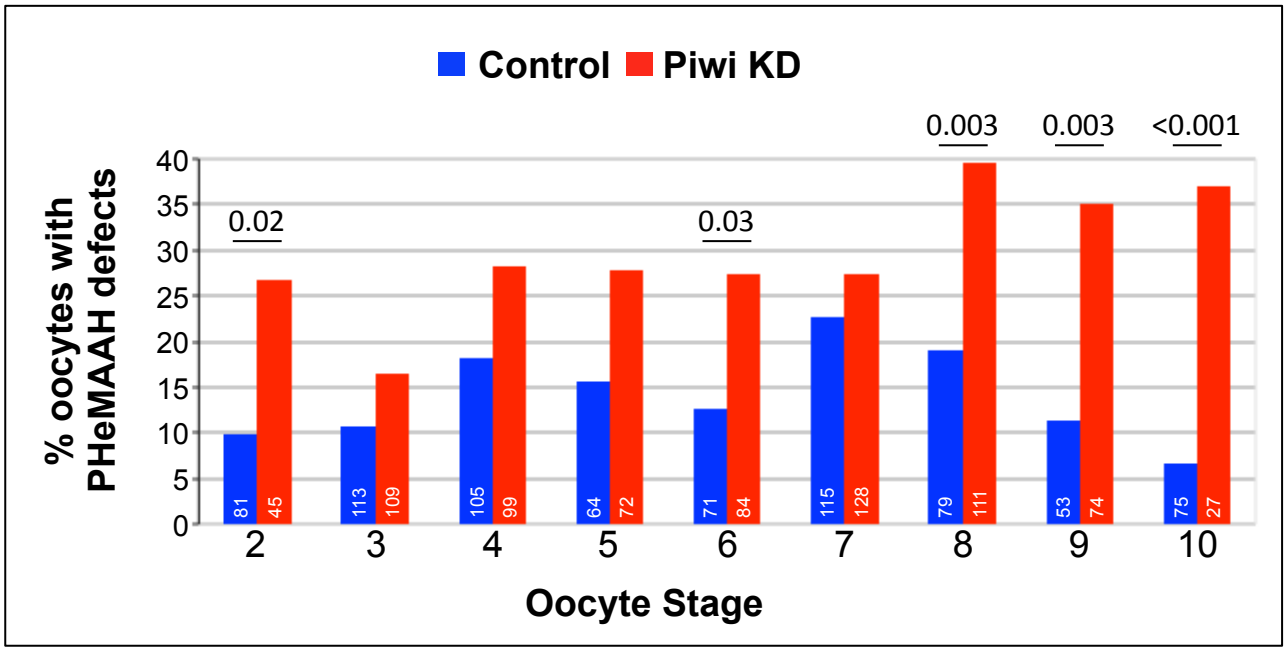

Figure S4. In both HP1a and Piwi KD ovarioles, PHeMAAH defects are more pronounced at later stages of oocyte development. The data from multiple FISH experiments (150 ovarioles for ea ch genotype) were pooled and tabulated for different stages of oogenesis. The developmental st age of each egg chamber was determined based on size and morphology (ASHBURNER *et al.* 2005). The number of oocytes scored is shown in white. P values are presented above the bars for those stages in which the difference between control and KD is statistically significant ($P < 0.05$). For complete data, see Table S4. (A) Data from HP1a RNAi^{V20} knockdown experiments. (B) Data from Piwi RNAi$^{V20\text{-}1}$ knockdown experiments.

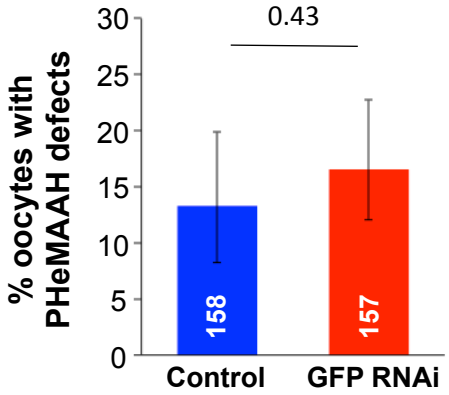

Figure S5. PHeMAAH defects do not arise from expression of an unrelated hairpin. To rule out the possibility that expression of any RNAi hairpin in the female germline could cause PHeMAAH defects, we used the matα driver to express a GFP RNAi hairpin in flies that lack a GFP transgene. FISH analysis was performed on *FM7a/X* oocytes in which GFP hairpin expression was induced (GFP RNAi) and those carrying the GFP RNAi transgene but no driver (Control). Number of oocytes assayed for each genotype is presented in white. 30 ovarioles of each genotype were scored. The P value is shown above the bars. For complete data, see Table S3.

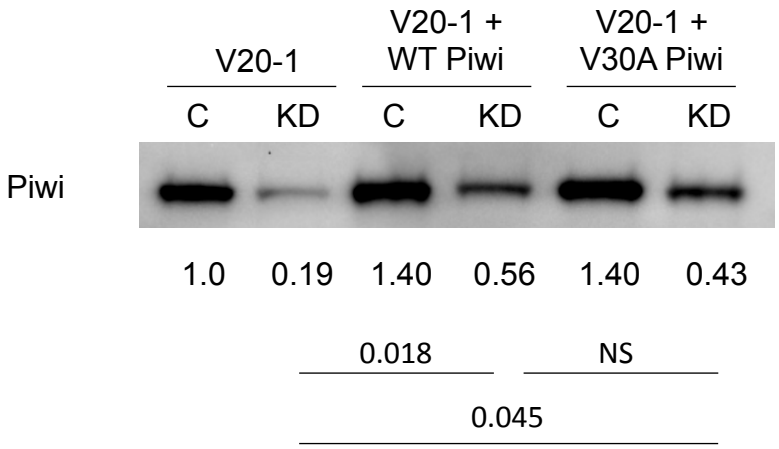

Figure S6. Expression of WT or V30A transgenic Piwi increases the level of Piwi protein when the Piwi RNAi$^{V20\text{-}1}$ hairpin is expressed. An immunoblot containing ovary extracts from flies harboring the Piwi RNAi$^{V20\text{-}1}$ hairpin and either no transgenic Piwi (V20-1), a wild-type transgenic copy of Piwi (V20-1 + WT Piwi), or a V30A Piwi transgene (V20-1 + V30A) is presented. Control (C) genotypes lack the matα driver, while in knockdown (KD) genotypes, matα induces expression of the hairpin. The signal intensity of each Piwi band was normalized to the total amount of protein/lane on the blot (using Bio-Rad Stain-Free technology). The numbers immediately below each lane represent mean normalized Piwi band intensity relative to the V20-1 control band. Presented values are averages from two independent experiments. Unpaired *t* test P values are presented for the indicated comparisons (NS = not significant).

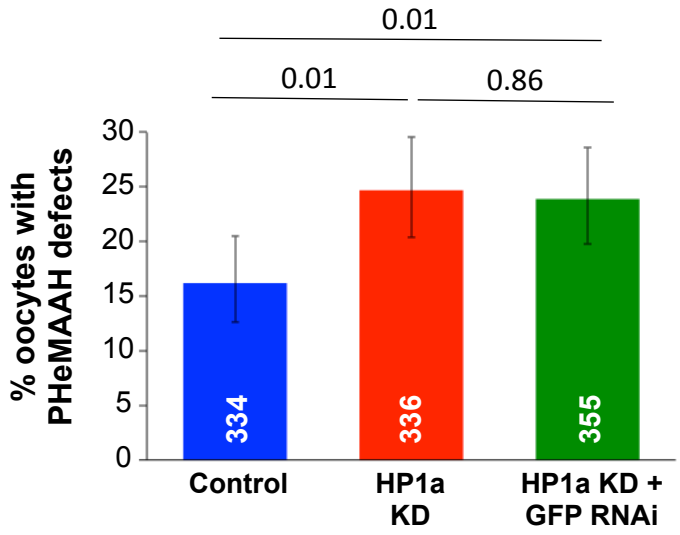

Figure S7. The presence of two UASi controlled transgenes does not cause detectable titration of Gal4 protein produced by the matα driver. Most of our FISH experiments utilized flies in which a single copy of the Gal4 driver induced expression of a single UAS-transgene, the RNAi hairpin. However, to look for rescue of PHeMAAH defects in HP1a KD oocytes, we utilized a single copy of the Gal4 driver to simultaneously drive two UAS transgenes: the RNAi hairpin and the UAS-GFP-HP1a construct. This raised the possibility that Gal4 levels might be insufficient to induce full expression of both constructs. If this were the case, reduced HP1a hairpin expression could result in fewer PHeMAAH defects, which would be misinterpreted as "rescue." To test this possibility, we performed an experiment to test for Gal4 titration. We used a single copy of the matα Gal4 driver to express the HP1a RNAi^{V20} hairpin as well as a GFP-hairpin in flies lacking a GFP transgene. Using FISH to assay PHeMAAH defects, we compared *FM7a/X* oocytes expressing both hairpins (HP1a KD + GFP RNAi) to those expressing only the HP1a hairpin (HP1a KD). PHeMAAH defects were comparable in both genotypes, and significantly more prevalent than in flies containing both hairpin transgenes but lacking a driver (Control). Numbers of oocytes scored for each genotype are presented in white. 60 ovarioles were scored per genotype. P values are shown above the bars. Complete data are presented in Table S3.

TABLE S1. LIST OF FLY STOCKS USED.

Genotype	Hairpin ID	Vector	Abbrevi-ation	Source	Bickel Stock #
DRIVER					
FM7a/y^{+}Y ; + ; P{w^{+mC}= matalpha4-GAL4-VP16} V37				Bickel lab derivative of T-273	T-600
RNAI TRANSGENES					
*y^{1} sc^{1} v^{1} ; + ; P{$y^{+t7.7}$ $v^{+t1.8}$=TRiP.**Su(var)205**. HMS00278} attP2*	SH00583.N	Valium 20	HP1a RNAi^{V20}	TRiP #33400	H-005
*y^{1} sc^{1} v^{1} ; + ; P{$y^{+t7.7}$ $v^{+t1.8}$=TRiP.**Su(var)3-9**. HMS00279} attP2*	SH00585.N	Valium 20	Su(var)3-9 RNAi^{V20-1}	TRiP #33401	H-031
*y^{1} sc^{1} v^{1} ; + ; P{$y^{+t7.7}$ $v^{+t1.8}$=TRiP.**Su(var)3-9**. HMS00704} attP2*	SH00979.N	Valium 20	Su(var)3-9 RNAi^{V20-2}	TRiP #32914	H-032
*y^{1} sc^{1} v^{1}; P{$y^{+t7.7}$ $v^{+t1.8}$=TRiP.**Eggless**. HMS00443}attP2*	SH00952.N	Valium 20	Eggless RNAi^{V20-1}	TRiP #32445	H-093
*y^{1} sc^{1} v^{1}; P{$y^{+t7.7}$ $v^{+t1.8}$=TRiP.**Eggless**. HMS00112}attP2*	SH00343.N	Valium 20	Eggless RNAi^{V20-2}	TRiP #34803	H-096
*y^{1} sc^{1} v^{1} ; + ; P{$y^{+t7.7}$ $v^{+t1.8}$=TRiP.**Piwi**. HMS00185} attP2*	SH00477.N	Valium 20	Piwi RNAi^{V20-1}	TRiP #34866	H-035
*y^{1} sc^{1} v^{1} ; + ; P{$y^{+t7.7}$ $v^{+t1.8}$=TRiP.**Piwi**. HMS00606} attP2*	SH00951.N	Valium 20	Piwi RNAi^{V20-2}	TRiP #33724	H-036
*y^{1} sc^{1} v^{1} ; P{$y^{+t7.7}$ $v^{+t1.8}$=TRiP.**EGFP**} attP40*		Valium 20	GFP RNAi^{V20}	Bloomington #41559	B-069
*w; P{VDRC.UAS-**HP1a** RNAi, w^{+}}*	12524		HP1a RNAi^{GD}	VDRC #31995	V-027
ADDITIONAL TRANSGENES					
*w^{1118}; P{w^{+mC} **GFP-HP1a**}/TM6b, Tb^{1}*				Bloomington #30561	B-067
*w^{1118}, P{**Piwi**^{WT}, w^{+mC}}*				Elgin lab	OL-092
*w^{1118}, P{**Piwi**^{V30A}, w^{+mC}}*				Elgin lab	OL-091
*y w; P{w^{+mC} **UAST-EGFP-HP1a [WT]** y^{+}} attP40*		pUAST	WT GFP-HP1a	This study	T-690
*y w; P{w^{+mC} **UAST-EGFP-HP1a [W200A]** y^{+}} attP40*		pUAST	W200A GFP-HP1a	This study	T-705
RNAI + PROTEIN TRANSGENES					
*w; P{VDRC.UAS-**HP1a** RNAi, w^{+}}; P{w^{+mC} GFP-HP1a}*	12524			This study	T-655
*w; P{w^{+mC} **UAST-EGFP-HP1a[WT]** attP40 y^{+}}; P{$y^{+t7.7}$ $v^{+t1.8}$=TRiP. **HP1a**. HMS00278} attP2*	SH00583.N			This study	T-719
*w; P{w^{+mC} **UAST-EGFP-HP1a[W200A]**attP40 y^{+}}; P{$y^{+t7.7}$$v^{+t1.8}$=TRiP. **HP1a**. HMS00278} attP2*	SH00583.N			This study	T-721

*w^{1118}, P{**Piwi^{WT}**, w^{+mC}}; P{$y^{+t7.7}$ $v^{+t1.8}$=**Piwi** TRiP.HMS00185} attP2/TM3, Sb*	SH00477.N			This study	T-714
*w^{1118}, P{**Piwi^{V30A}**, w^{+mC}}; P{$y^{+t7.7}$ $v^{+t1.8}$=**Piwi** TRiP.HMS00185} attP2/TM3, Sb*	SH00477.N			This study	T-713
HP1A MUTANT STOCK					
y/y^{+} Y;Su(var)205^{5}/SM1				Bickel lab derivative of Bloomington #6234	M-828
OTHER					
FM7a				Bickel lab	A-195
w^{1118} B^{1}				Bickel lab	W-097
C(1)RM,y^{2},su(w^{a}) w^{a} / X^Y,vfB				Bloomington #700	C-200
C(1)M4, y^{2} / C(1;Y)6, w^{1118}				Bloomington #1999	C-217

TABLE S2. PRIMERS USED IN CONSTRUCTION OF GFP-HP1A CONSTRUCTS.

Name	**Sequence (5' – 3')**
Mutagenesis Primers	
GFP KpnI F	CTGCAGTCGACGGAACCGCGGGCCCGGG
GFP KpnI R	CCCGGGCCCGCGGTTCCGTCGACTGCAG
GFP Xba F	GCCCGGGATCGACCGGATCCAGATAACTGATCATAATCAG
GFP Xba R	CTGATTATGATCAGTTATCTGGATCCGGTCGATCCCGGGC
GFP Bam2 F	GGGATCGACCGGATCGAGATAACTGATCATAATCAG
GFP Bam2 R	CTGATTATGATCAGTTATCTCGATCCGGTCGATCCC
W200A F	CACTTCTACGAAGAGCGCCTATCCGCGTACTCTGATAATG
W200A R	CATTATCAGAGTACGCGGATAGGCGCTCTTCGTAGAAGTG
Cloning Primers	
GFP clon F	ATCGGGTACCAAAATGGTGAGCAAGGGCGAGG
GFP clon4 R	ATCGACTAGTGCCGCCTCTCGATCCGGTCGATCCC
HP1a clon2 F	ATCGACTAGTGGCAAGAAAATCGACAACCC
HP1a clon R	ATCGGGATCCGATCCAACCTGTTTAATCTTCATTATC
Sequencing Primers	
pUAST Seq 5'	CGCAGCTGAACAAGCTAAAC
pUAST Seq 3'	TGCTCCCATTCATCAGTTCC
pUASP Seq 5'	GGCAAGGGTCGAGTCGATAG
pUASP Seq 3'	AGGTTTAACCAGGGGATGCT
pGFPSeq F	CGTGTACGGTGGGAGGTCTA
pGFPSeq R	GGGAGGTGTGGGAGGTTTT
GFPSeq2 F	TAAGCAGAGCTGGTTTAGTG
GFPSeq2 R	GCATTCATTTTATGTTTCAGG

TABLE S3. COMPLETE GENOTYPES AND DATA FOR FISH EXPERIMENTS PRESENTED IN FIGURES 1, 3, 4, S5, AND S7.

Fig	Hairpin ID	Genotype	# ovar-ioles	# normal PHeMAAH	# defective PHeMAAH	% defective PHeMAAH
				Oocytes		
1D	GD	**C:** *FM7a/y w; HP1a RNAi^{GD}/+; GFP-HP1a/+*	60	249	39	13.5
1D	GD	**KD:** *FM7a/y w; HP1a RNAi^{GD}/+; matα /+*	60	213	60	22.0
1D	GD	**KD + HP1a:** *FM7a/w; HP1a RNAi^{GD}/+; GFP-HP1a/matα*	60	258	43	14.3
1D	V20	**C:** *FM7a/y sc v; HP1a RNAi^{V20}/+*	90	337	42	11.1
1D	V20	**KD:** *FM7a/y sc v; HP1a RNAi^{V20}/matα*	90	281	89	24.0
1E	V20-1	**C:** *FM7a/y sc v; Su(var)3-9 RNAi$^{V20\text{-}1}$/+*	30	119	16	11.9
1E	V20-1	**KD:** *FM7a/y sc v; Su(var)3-9 RNAi$^{V20\text{-}1}$/ matα*	30	109	30	21.6
1E	V20-2	**C:** *FM7a/y sc v; Su(var)3-9 RNAi$^{V20\text{-}2}$/+*	60	252	34	11.9
1E	V20-2	**KD:** *FM7a/y sc v; Su(var)3-9 RNAi$^{V20\text{-}2}$/ matα*	60	242	64	20.9
1F	V20-1	**C:** *FM7a/y sc v; Eggless RNAi$^{V20\text{-}1}$/+*	60	280	44	13.6
1F	V20-1	**KD:** *FM7a/y sc v; Eggless RNAi$^{V20\text{-}1}$/matα*	60	270	76	22.0
1F	V20-2	**C:** *FM7a/y sc v; Eggless RNAi$^{V20\text{-}2}$/+*	60	268	45	14.4
1F	V20-2	**KD:** *FM7a/y sc v; Eggless RNAi$^{V20\text{-}2}$/matα*	60	239	95	28.4
3B	V20-1	**C:** *FM7a/y sc v;Piwi RNAi$^{V20\text{-}1}$/+*	60	269	40	12.9
3B	V20-1	**KD:** *FM7a/y sc v;Piwi RNAi$^{V20\text{-}1}$/matα*	60	200	84	29.6
3B	V20-2	**C:** *FM7a/y sc v;Piwi RNAi$^{V20\text{-}2}$/+*	30	135	24	15.1
3B	V20-2	**KD:** *FM7a/y sc v;Piwi RNAi$^{V20\text{-}2}$/matα*	30	131	46	26.0
3C	V20-1	**C:** *FM7a/y sc v;Piwi RNAi$^{V20\text{-}1}$/+*	90	382	70	15.5
3C	V20-1	**KD:** *FM7a/y sc v;Piwi RNAi$^{V20\text{-}1}$/matα*	90	334	133	28.5
3C	V20-1	**KD+WT:** *FM7a/w, Piwi[WT]; Piwi RNAi$^{V20\text{-}1}$/ matα*	90	376	89	19.1
3C	V20-1	**KD+V30A:** *FM7a/w, Piwi[V30A]; Piwi RNAi$^{V20\text{-}1}$/matα*	90	352	132	27.3
4B	V20	**C:** *FM7a/w;HP1a RNAi^{V20}/+*	60	270	55	16.9
4B	V20	**KD:** *FM7a/w;HP1a RNAi^{V20}/matα*	60	261	89	25.4
4B	V20	**KD+ WT:** *FM7a/w; GFP-HP1a[WT]/+; HP1a RNAi^{V20}/matα*	60	284	61	17.7
4B	V20	**KD+W200A:** *FM7a/w; GFP-HP1a[W200A]/+; HP1a RNAi^{V20}/matα*	60	263	94	26.3
S5	V20	**C:** *FM7a/y sc v; GFP RNAi/+*	30	137	21	13.3
S5	V20	**KD:** *FM7a/y sc v; GFP RNAi/+;matα/+*	30	131	26	16.6
S7	V20	**C:** *FM7a/w; GFP RNAi/+; HP1 RNAi^{V20}/+*	60	280	54	16.2
S7	V20	**HP1 KD:** *FM7a/w; +/+; HP1a RNAi^{V20}/matα*	60	253	83	24.7
S7	V20	**HP1a+GFP KD:** *FM7a/w; GFP RNAi/+; HP1a RNAi^{V20}/matα*	60	270	85	23.9

TABLE S4. COMPLETE DATA FOR STAGE-BY-STAGE FISH ANALYSES PRESENTED IN FIGURE S4.

A: HP1a stage-by-stage analysis (150 ovarioles)						
	Control: *FM7a/X; HP1a RNAi^{V20}/+*			**KD:** *FM7a/X; HP1a RNAi^{V20}/matα*		
Stage	# normal PHeMAAH	# defective PHeMAAH	% defective PHeMAAH	# normal PHeMAAH	# defective PHeMAAH	% defective PHeMAAH
2	36	1	2.7	37	10	21.3
3	89	6	6.3	75	15	16.7
4	62	20	24.4	63	27	30.0
5	56	8	12.5	67	14	17.3
6	65	16	19.8	56	17	23.3
7	103	20	16.3	79	41	34.2
8	81	18	18.2	87	21	19.4
9	56	6	9.7	28	12	30.0
10	58	2	3.3	49	17	25.8

B: Piwi stage-by-stage analysis (150 ovarioles)						
	Control: *FM7a/X; Piwi RNAi^{V20-1}/+*			**KD:** *FM7a/X; Piwi RNAi^{V20-1}/matα*		
Stage	# normal PHeMAAH	# defective PHeMAAH	% defective PHeMAAH	# normal PHeMAAH	# defective PHeMAAH	% defective PHeMAAH
2	73	8	9.9	33	12	26.7
3	101	12	10.6	91	18	16.5
4	86	19	18.1	71	28	28.3
5	54	10	15.6	52	20	27.8
6	62	9	12.7	61	23	27.4
7	89	26	22.6	93	35	27.3
8	64	15	19.0	67	44	39.6
9	47	6	11.3	48	26	35.1
10	70	5	6.7	17	10	37.0